published online 15 JAN 2008

Dust Separation

ULLMANN'S ENCYCLOPEDIA OF INDUSTRIAL CHEMISTRY

Eberhard Schmidt, Bergische Universität Wuppertal, Wuppertal, Germany

Symbols

a:	plate spacing, tube radius
A:	surface area
b:	specific scrubbing liquor ratio
c:	particle concentration
c_m:	limiting dust load
C_D:	drag coefficient
d_G:	diameter of granules
d_l:	droplet diameter
D_F:	fiber diameter
e:	diameter of flow tube
E:	overall collection efficiency
f:	circular cross-sectional area
f:	factor
f':	fitting parameter
F:	filtration area
h:	adhering fraction
H:	height
k_1 k_2:	fitting parameters
k_a, k_b:	fitting parameters
K_1:	residual resistance of filter medium after cleaning
K_2:	specific resistance of filter cake
L:	collection length
m:	specific cleaned volume
m:	particle mass
M:	filter mass per unit filter area
$\dot{M}$:	mass flow rate
n:	empirical fitting factor
N:	number of cyclones
Δp:	pressure drop
P:	penetration
q (x):	particle-size distribution
r:	radius

DOI: 10.1002/14356007.b02_13.pub2

R: resultant of external forces
Re: Reynolds number
t: time
T: absolute temperature
$T(x)$: fractional collection efficiency
U_0: gas velocity, superficial velocity
v: velocity
v: air to cloth ratio
v_{rel}: relative velocity between the droplet and the gas
$\dot{V}$: volume flow rate
w: particle velocity
$w(x)$: migration velocity
W: mass of dust deposited per unit filter area
x: particle size (diameter)
x_{cr}: critical particle diameter
x_t: cut size
Z: thickness
ε: porosity
η: collision efficiency
η: transport parameter
μ: dynamic viscosity
μ_m: maximum dust load
ξ: pressure-drop coefficient
ϱ_g: gas density
ϱ_F: fiber density
φ: collection efficiency of single fiber or granule
ψ: inertial (Stokes) parameter

Subscripts

c: collected
D: diffusion
e: entry
f: fine
F: fiber
g: gas
i: internal
l: scrubbing liquor
p: particle
r: radial
φ: tangential

1. Introduction

Whether desired or not, many industrial processes inevitably generate particles entrained by a carrier gas. These particles may be solid (dust) or liquid (droplets or mist). As a rule, the particles must be separated from the transporting gas, either because they are the desired product or because they are an undesirable or even harmful emission.

Product recovery by means of dust (gas–solid) separation has been practiced long and intensively in process engineering. The importance of emission control has grown, and standards have become more stringent. Rapid increases in industrial production and a better knowledge of potential hazards and harmful effects have led to more stringent regulations for the control of air pollution. One example is the emission limits established in "TA Luft 2002" [9], an administrative regulation issued by the Federal Republic of Germany, which tolerates a maximum emission of 20 mg/m^3 of inert dust only. In many cases, which are defined in these regulations, the specified emission value is much lower than this. For dust that is harmful to health, the limits are geared to the potential hazard and run from 1 mg/m^3 (e.g., antimony, chromium), through 0.5 mg/m^3 (e.g., lead, nickel), to 0.05 mg/m^3 (e.g., mercury, thallium). In future these will be supplemented by regulations concerning particle size classes (PMx).

Because dust concentration upstream of collection equipment is frequently in the range of 1 – 10 g/m^3, collection efficiencies greater than 99.99 % are often necessary to meet the above limits. Such values can be achieved only through the most painstaking selection and design and, in many cases, only by combining several types of equipment. One difficulty is that the size distribution of the particles to be collected generally extends over a wide range, from < 0.1 µm to > 100 µm; the harmful components (e.g., heavy metals), which demand especially efficient collection, often fall in the fine range below 1 µm.

Dust collection methods used in practice can be classified as

1. Inertial and centrifugal separation (gas cyclones)
2. Wet collection (scrubbers)

3. Filtration (fibrous filters, fabric filters, granular-bed separators, etc.)
4. Electrostatic collection (precipitators).

All of these collectors separate particles from gas by a common principle: forces acting on the particles cause them to enter regions from which the gas cannot transport them away. These regions may be the inner wall of a cyclone, the droplet surface in a scrubber, the fiber or grain surface in a filter, or the collecting electrode in a precipitator.

An elementary theory of gas–solid separation thus consists of calculating particle trajectories by solving the equation of motion:

$$m \cdot \mathrm{d}w/\mathrm{d}t = R \tag{1}$$

where m is the particle mass, w is the particle velocity, t is time, and R is the resultant of the external forces acting on the particle (such as gravitational, hydrodynamic and electrical forces).

As a rule, Equation (1) is solved numerically. A problem arises because the flow field of the gas must be entered into the equation and this field is often not known precisely. Furthermore, a random component of motion may also be involved, allowance for which can be difficult. In practice, therefore, approximations are used or a purely empirical approach is taken, in which design is based on experimental findings for a given type of equipment. The drawback of the empirical method is that the extent to which experience can be extrapolated to new situations is unclear.

2. Evaluation of Dust Collection Equipment

To evaluate dust collection equipment, both the energy consumption (or pressure drop Δp) and the collection efficiency must be determined. The latter can be found by integral techniques (for the totality of particles) or differential methods (for each size fraction).

A general plan for characterizing a separation can be found in DIN ISO 9276-4 [10]. Here, only the case is considered where the solid material entering along with the crude gas is assumed to be separated into two components. The nomenclature has been adapted to common usage in separation technology; important parameters are depicted and defined in Figure 1.

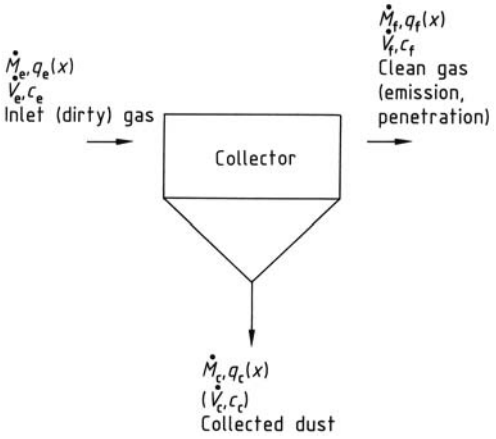

Figure 1. Notation used in dust collectors
M = mass flow rate of particles; V = volume flow rate of gas; c = particle concentration; q (x) = particle-size distribution (density distribution)
Subscripts: c = collected (coarse); e = entry (inlet); f = fine (penetrating)

The *overall collection efficiency* (integral mass balance) E, also known as the total or cumulative collection efficiency, is given by

$$E = \frac{\dot{M}_c}{\dot{M}_e} \tag{2a}$$

or

$$E = 1 - \frac{\dot{M}_f}{\dot{M}_e} \tag{2b}$$

In view of the importance of emissions, especially for collection efficiencies close to 100 %, the *penetration* P is more informative:

$$P = 1 - E \tag{3}$$

or

$$P = \frac{\dot{M}_f}{\dot{M}_e} \tag{4}$$

As a rule, dust loads upstream and downstream of the collection equipment are measured experimentally and E is determined as follows:

$$E = \frac{\dot{V}_e c_e - \dot{V}_f c_f}{\dot{V}_e c_e} \tag{5}$$

with $\dot{V}_e = \dot{V}_f$, then

$$E = 1 - \frac{c_f}{c_e} \tag{6}$$

or

$$P = \frac{c_f}{c_e} \tag{7}$$

Note that, if a collection device is rated in terms of overall collection efficiency, this quantity depends not only on the equipment design and operating conditions, but also on the type of dust and, especially, the particle-size distribution. The stated overall collection efficiency or overall penetration thus always refers to a particular case; this severely restricts its applicability to other situations.

A more useful and informative measure is the *fractional collection efficiency,* also called the "grade efficiency," "separation efficiency," or "separation function." The fractional collection efficiency $T(x)$ measures collection as a function of particle size, x; it is defined as

$$T(x) = \frac{d\dot{M}_c(x)}{d\dot{M}_e(x)} = 1 - \frac{dc_f(x)}{dc_e(x)} \tag{8}$$

Hence,

$$T(x) = 1 - \frac{Pq_f(x)}{q_e(x)} \tag{9a}$$

or

$$T(x) = \frac{Eq_e(x)}{q_e(x)} \tag{9b}$$

Procedures for measuring $T(x)$ are based on Equations (9a) and (9b); Equation (9a) is employed most commonly in separation technology.

Typical fractional collection curves are presented in subsequent chapters on individual types of collection equipment. The *cut size* x_t is the particle size at which a given fractional collection efficiency is achieved. A value of 50 % is often used ($x_{50,\,t}$) but other cut sizes (e.g., $x_{90,\,t}$, $x_{99,\,t}$) may be chosen depending on technical requirements and specific applications.

One advantage of the fractional collection efficiency is that, being a ratio, it is independent of the quantity (e.g., number or mass) used to express the amount of particulate material in the particle-size ranges upstream and downstream from the collection equipment. The fractional collection efficiency is a property of the apparatus and can thus be used to estimate the expected overall collection efficiency for any given particle size distribution; this is important in the selection and sizing of dust collectors:

$$E = 1 - P = \int_{x_{min}}^{x_{max}} T(x) \cdot q_e(x) dx \tag{10}$$

The overall collection efficiency calculated by means of Equation (10) is, of course, expressed in the same quantity as the particle-size distribution of the inlet gas $q_e(x)$; it is usually a mass fraction but can also be a number fraction.

3. Centrifugal Collectors (Cyclones)

3.1. General

The simplest way to separate particles from gases is to allow them to settle out in so-called gravity settlers into zones of low gas velocity [11]. Because this method is technically feasible only for coarse particles that are significantly larger than 100 μm, gravity settlers now have negligible importance and are not discussed here.

Even before the end of the 19th century, collection by means of centrifugal forces was known to be much more efficient than simple gravity separation. This led to the development of centrifugal collectors; the most commonly used form employs flow reversal and is called a gas cyclone.

Because of their simple design, reliable operation, small space requirement, and low cost, cyclones are used widely in many branches of industry. They are frequently employed in material recovery from gas recycle systems, pneumatic conveying, and other areas.

Cyclones can be operated at pressures of 0.001 – 10 MPa and temperatures exceeding 1200 °C. They currently provide the most common method of particle collection at high temperature (> 1000 °C) for use on an industrial scale. Growing interest in dust removal from hot gases has given a new impetus to research and development work on cyclones [12].

The advantages of cyclones over other collectors are offset by the fact that they are less efficient collectors for particles below ca. 1 – 5 μm in size. Therefore, in view of the

increasingly stringent requirements on collecting capacity, the use of cyclones is restricted; they are often used as first-stage collectors (precollectors).

3.2. Mode of Operation and Basic Designs

Figure 2 shows the most common type of cyclone with flow reversal. The gas path is designed to impart a twist to the particle-laden gas entering the rotationally symmetrical apparatus. A turbulent, three-dimensional, rotational flow is produced. In the separating chamber spiral, downward flow takes place at larger radii. Flow is then reversed, and the gas spirals upward at smaller radii, and reaches the exit duct. The particles entrained in the revolving gas stream experience centrifugal forces hundreds to thousands of times greater than the force of gravity. Thus, the larger particles migrate outward to the cyclone wall, where they collect as strands; they are carried downward along the tapered body and out of the separating chamber by boundary-layer flow. The conical shield (d), often built into the bottom of the tapered body, prevents already collected material from being reentrained. The particles that are not collected are carried inward by the gas flow and removed through the exit duct (vortex finder).

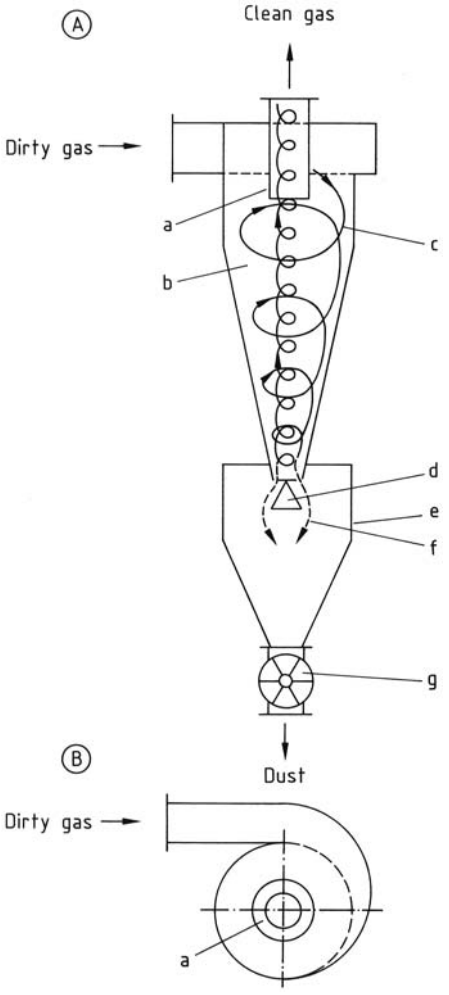

Figure 2. Schematic of a reverse-flow cyclone A) Vertical section; B) Top view
a) Exit duct; b) Separating chamber; c) Gas flow pattern; d) Conical shield; e) Dust hopper; f) Dust; g) Lock

Cyclones vary in the form of the swirl-producing inlet (tangential, axial with swirl vanes); the shape of the separating chamber (cylindrical, conical); the design of the exit duct; and their dimensions. Diameters range from 5 m to 2 cm (the latter for measurement purposes); flow rates vary from 1 to 100 000 m^3/h. Reviews of cyclone construction are given in [13, 14].

3.3. Design Calculations

Important parameters in cyclone design and operation are the fractional collection efficiency $T(x)$ (defined in Eq. 8) and the energy consumption, which is measured in terms of the pressure drop Δp.

3.3.1. Collection Efficiency

In theory, particle trajectories inside the cyclone can be calculated to determine the fractional collection efficiency; such calculations have been attempted [15, 16]. This method provides insight into processes occurring in the cyclone which improve the understanding of particle separation. However, because the flow field is complicated and turbulence must be considered, this procedure is quite complex and not yet adequately proven. Thus far, it has been primarily of scientific interest and has not been used practically.

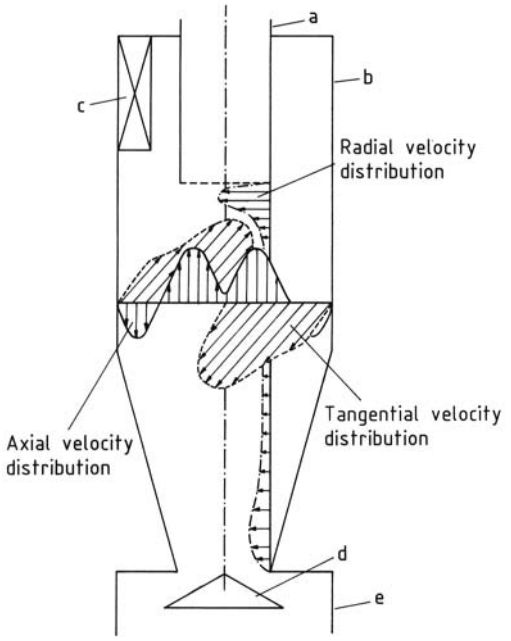

Figure 3. Flow field in a gas cyclone
a) Exit duct; b) Separating chamber; c) Gas inlet; d) Conical shield; e) Dust hopper

Models for Low Dust Loads. Several models have been devised for the approximate calculation of collection efficiency at low dust loads [17–23]. They describe the flow field in more or less simplified terms. The flow field is shown schematically in Figure 3. An especially important parameter is the tangential velocity component v_φ, which initially increases with decreasing radius and can be approximated in this region by

$$v_\varphi \cdot r^n = \text{constant} \tag{11}$$

Here r is the radius and n is an empirical exponent that takes into account the loss of angular momentum due to friction. In a loss-free vortex, n would be unity; in real gas flow, it lies between 0.5 and 0.8. The value of n depends on other factors, such as wall roughness, particulate load, and cyclone geometry [24].

Because of a strong "vortex" in the cyclone, the tangential velocity depends mainly on the radius and not on the height. In the core of the cyclone, the tangential component decreases rapidly and approaches zero at the axis.

Design models are based either on a residence-time concept [18] or a separation-zone concept [19, 20]. Approved theoretical work combines both concepts [21–23].

The separation-zone model proposed by Barth [19] and improved by Muschelknautz [20] is now employed widely because of its simplicity and ease of use. However, this approach does not give the complete fractional efficiency curve; only a *critical particle diameter* x_{cr} can be calculated [17]:

$$x_{cr} = \left[\frac{18\mu_g \cdot v_{r,i} \cdot r_i}{(\varrho_p - \varrho_g) \cdot v_{\varphi,i}^2}\right]^{\frac{1}{2}} \tag{12}$$

where μ_g is the dynamic viscosity of the gas, ϱ_p is the particle density, ϱ_g is the gas density, r_i is the internal radius of the exit duct, $v_{r,\,i}$ is the radial velocity at radius r_i, and $v_{\varphi,\,i}$ is the tangential velocity at radius r_i.

According to this concept, all particles whose diameter x is less than x_{cr} pass through the device; all particles with $x > x_{cr}$ are collected.

In theory, the fractional efficiency curve jumps from 0 to 1 at x_{cr} (curve a, Fig. 4). Barth assumed that x_{cr} corresponds to the median diameter $x_{50,\,t}$ of the separation function $T(x)$, i.e., the 50 % value on the effective S-shaped fractional efficiency curve (curve b, Fig. 4). On the basis of experimental results (curve c, Fig. 4), the suggestion has been made that the actual cut diameter be estimated as $x_{50,\,t} \approx 1.3\ x_{cr}$ [20].

Although using Equation (12) to predict the critical diameter involves some uncertainty and the complete fractional efficiency curve cannot be derived, experience shows that this formula has an important advantage: experimental values

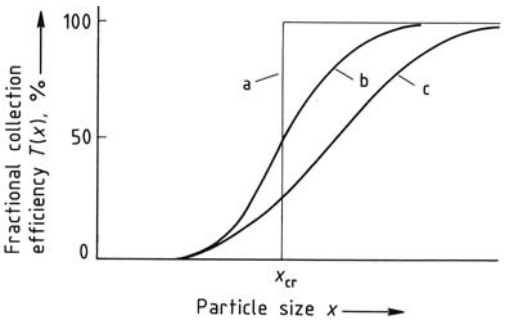

Figure 4. Fractional efficiency curves for cyclones
a) Theoretical cut diameter [19]; b) Assumed effective curve [19]; c) Experimental curve [20]

of x_{50} can be converted easily and reliably to different conditions, i.e., the change in the cut diameter produced by a change in cyclone geometry, gas velocity, or gas temperature (viscosity) can be estimated.

In a more detailed approach [22, 23], particle motion is treated as a process in which diffusional particle transport is superimposed on a predetermined motion. Particle flux calculations are based on a modified flow field [24]. The advantage of this model is that the complete fractional efficiency curve can be obtained and the entire cyclone geometry is allowed for. The computing time needed for numerical calculation is short, and processing can be done with an ordinary personal computer. Comparison has shown good agreement with measured values.

Models for High Dust Loads. The computational techniques described up to this point have all presumed that the particle concentration entering the cyclone is low and, therefore, has a negligible effect on flow conditions in the separating chamber. This is the case up to a particle load of ca. 10 g/m^3. In practice, however, cyclones often operate at higher concentration. Experiment has shown that the collection efficiency of a cyclone improves with increasing particulate load in the inlet gas, even though the tangential velocity (which is responsible for collection in the vortex) and the centrifugal acceleration decrease simultaneously.

At higher particle concentration, additional collection mechanisms contribute to particle separation, and these must also be taken into account in design.

By analogy with pneumatic conveying, MUSCHELKNAUTZ [20] reasons that a fluid stream can transport only a limited particle mass flow. If a limiting dust load c_m is exceeded, the excess particle mass is accelerated to the wall immediately after entering the cyclone and moves down into the dust trap in the form of a strand. Collection due to a dust load in excess of c_m is assumed to be selective only at low total loads and increasingly nonselective (i.e., independent of particle size) at higher loads. If c_m is exceeded and the particles thrown to the wall are collected in the inlet, the remaining particles can be collected selectively in the separating chamber. Thus, particle collection at high concentration can be considered as two consecutive processes. Equations for calculating the overall collection efficiency of a cyclone are given in [17, 25].

Along with particle collection due to excess loading, agglomeration of small particles with large ones can be assumed to occur at high particle concentration; this also improves overall collection efficiency. A model that takes account of agglomeration is described in [22, 26]. Larger particles migrate to the wall of the cyclone at a higher radial velocity than the small particles. This difference in settling velocity leads to collisions between particles of different sizes and hence to agglomeration. Separation of the small particles adhering to the larger ones is thus improved.

3.3.2. Pressure Drop

The total pressure drop Δp of a cyclone consists of pressure losses in the inlet, separating chamber, and exit duct; it is usually calculated as follows:

$$\Delta p = \xi \frac{\varrho_g}{2} v_i^2 \tag{13a}$$

where

$$\xi = \xi_{inlet} + \xi_{separator} + \xi_{exit} \tag{13b}$$

Here ξ is the pressure-drop coefficient, ϱ_g is the density of the gas, and v_i is the axial velocity in the exit duct.

The calculation of ξ is described in [17]. Experience has shown that the pressure drop in the exit duct accounts for as much as 90 % of the total cyclone pressure drop. Usually, ξ varies from 5 to 40, depending on cyclone geometry; values of 10 – 20 are common. Typical values for Δp are in the range of 500 – 2000 Pa.

The collection efficiency and the pressure drop depend on cyclone geometry and volume flow rate. These quantities can be combined and used to find the "optimum" cyclone with either a minimum pressure drop [27] or minimum equipment volume [20, 28] for a given cut diameter. Calculations of this kind are not always implemented, however, because they can yield unrealistically long cyclone designs, especially for fine particles. Empirical shapes are, therefore, generally used.

3.4. Operating Characteristics

The collection performance of a cyclone depends chiefly on its geometry, gas throughput, inlet gas concentration, and properties of the material to be separated. The change in cut size under different operating conditions can be estimated with Equation (12). For example, an increase in gas viscosity (e.g., when the temperature is raised) decreases performance. If the cyclone geometry is altered (e.g., exit-duct diameter or inlet cross section is diminished), the tangential velocity component $v_{\varphi,\,i}$ at the exit-duct radius increases so that a greater centrifugal force acts on the particles. As a result, the cut size $x_{50,\,t}$ decreases and particle collection improves.

Collection efficiency is also improved if the volume flow rate through the cyclone increases. Figure 5 shows some fractional efficiency curves for an experimental cyclone in which the inlet velocity v_e, and thus the volume flow rate $\dot{V}$ are varied. The cut size decreases with increasing $\dot{V}$. The following relation between cut size and gas throughput can be derived from Equation (12):

$$x_{50,t} \sim \frac{1}{\sqrt{\dot{V}}} \tag{14}$$

When the tangential velocity in the cyclone increases, however, the pressure drop Δp also increases. To achieve good collection performance and acceptable energy consumption when gases with high flow rates have to be cleaned,

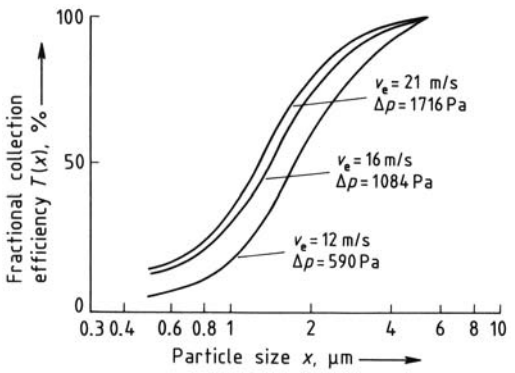

Figure 5. Fractional efficiency curves for a cyclone at various inlet velocities v_e and pressure drops Δp
Particle concentration = 0.5 g/m^3; external radius of cyclone = 95 mm; radius of exit duct = 37 mm; cyclone height = 612 mm; cross-sectional area of inlet duct = 0.003 m^2

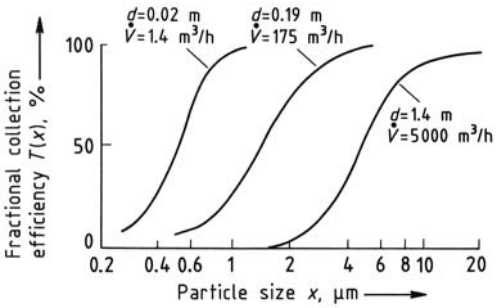

Figure 6. Fractional efficiency curves for cyclones of varying diameter d at a constant pressure drop
$\dot{V}$ = volume gas flow rate

several small cyclones connected in parallel are preferable to a large cyclone because the reduction in cyclone diameter shifts the cut size toward smaller particle sizes. Figure 6 presents typical fractional efficiency curves for three cyclones with different diameters but the same pressure drop (the gas flow rate $\dot{V}$ decreases at the smaller diameters). Cleaning a gas with a given flow rate, therefore, requires more cyclones as the cyclone diameter decreases. If geometrically similar cyclones are assumed and Δp is constant, the result of Equations (12) and (13a), (13b) is that the cut size for N cyclones in parallel decreases in proportion to $(1/N)^{1/4}$.

Systems composed of many small cyclones are often called *multicell collectors* or *multicyclones.* An example is shown in Figure 7.

Cyclones with diameters of a few centimeters and particle cut sizes less than 1 µm are used mainly for testing and measuring purposes rather than industrial dust collection.

Substantial differences are often found between calculated and measured collection efficiencies. This discrepancy occurs because the cyclone design is unsuitable for the internal flow pattern and, thus, unfavorable for collection.

An especially important point is the correct design of the dust removal system. Long vertical tubes have proved valuable, as have conical shields which must be mounted below the cyclone cone. The cyclone should not be too long, and the ratio of the dust discharge opening area to the exit-duct cross-sectional area should be greater than one; this prevents the inner vortex core from being deflected toward the wall and reentraining already collected particles.

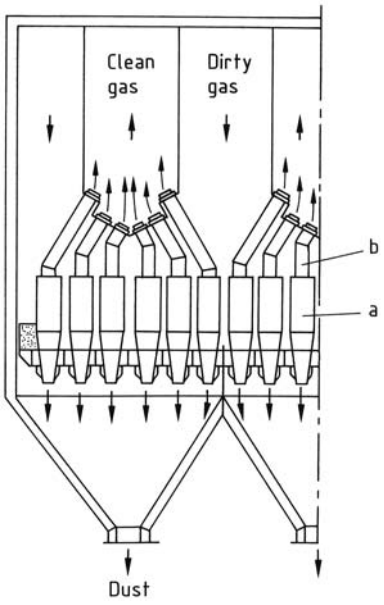

Figure 7. Multicyclone (Lurgi, Multiklon) with bent clean-gas pipes
a) Separating cell; b) Clean-gas pipe

In multicell collectors, the cells should be loaded uniformly; short-circuit flow at the dust removal ends of the cells leads to poorer separation and must be prevented.

Finally, no welded joints or other flow-obstructing ridges should protrude into the cyclone. Such irregularities can yield secondary flow patterns that reduce collection performance. Detailed information on cyclone design can be found in [29].

4. Scrubbers

4.1. General

In wet collectors (scrubbers), both particulate and gaseous components can be separated from the carrier gas. Only particle collection is discussed below; for gas separation see → Absorption, 1. Fundamentals.

Even very fine particles (≤ 0.1 μm) can be collected in scrubbers. The particles are brought into contact with a scrubbing liquor, generally water; they bind to the liquor and are removed from the gas stream in bound form as a slurry. Thus two operations must take place in a scrubber: (1) incorporation (binding) of particles into the scrubbing liquor and (2) separation of the dust-laden liquor. In most scrubbers, especially those with the best collection efficiency for fine particles, the scrubbing liquor is in droplet form. The first operation can, therefore, be regarded as the agglomeration of (small) solid particles and (larger) liquid particles. These larger droplets are readily collected from the gas stream. However, care must be taken to ensure the efficient separation of dust-laden liquid droplets, especially in high-energy scrubbers which use relatively fine droplets.

Scrubbers are relatively easy to adapt to various operating conditions. They are employed mainly when products are to be recovered from a wet phase or when the danger of dust explosion or other hazards forbids dry collection. They have proved suitable chiefly for moderately large-volume gas flow rates (often $< 30\ 000\ m^3/h$).

The solid materials collected in scrubbers are transferred from a gas into a liquid, usually water; therefore, their use entails either wastewater treatment (which may also be dictated by the presence of absorbed gases such as hydrogen chloride or fluorine) or recycling of the scrubbing liquor in the plant. In either case, water consumption has to be minimized by setting up a closed liquor cycle and optimizing collection conditions. Finally, the danger of corrosion or icing should be mentioned.

4.2. Mode of Operation and Basic Designs

Many scrubber designs are available; examples can be found in [30–33]. However, most designs fall into five basic types, shown in Figure 8.

The *spray tower* (Fig. 8 A) is the oldest type of scrubber. The dirty gas flows upward through a large tube at a relatively low speed of ca. 1 m/s. The washing fluid is dispersed countercurrent to the gas by spray nozzles that are mounted at different levels. The dust-laden liquid leaves the bottom of the scrubber. Packings, e.g., glass beads, are sometimes used to improve collection efficiency (packed-bed scrubbers). In any case, a droplet separator must be integrated in the clean-gas duct.

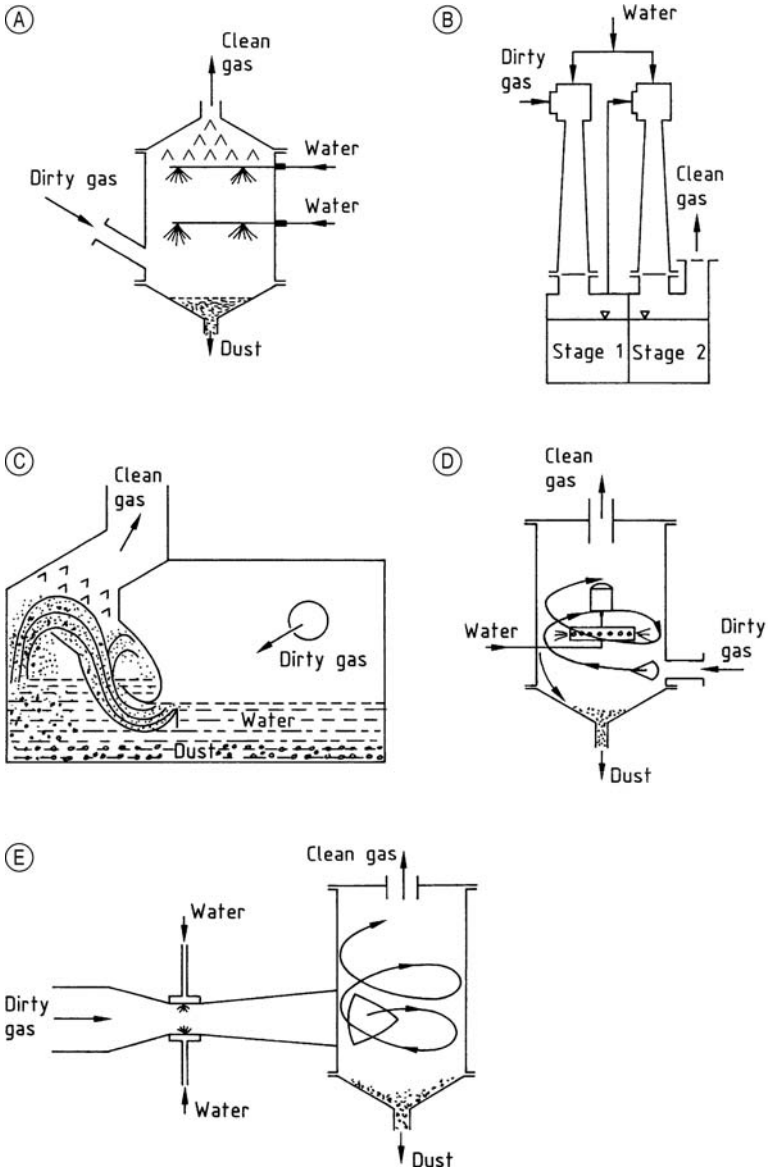

Figure 8. Basic types of scrubbers
A) Spray tower; B) Ejector venturi scrubber; C) Self-induced spray scrubber; D) Rotational scrubber; E) Venturi scrubber

The *ejector venturi scrubber* (Fig. 8 B) is basically a water-jet pump. Water is sprayed into the scrubber at a speed of ca. 25 – 35 m/s and provides a draft for moving the gas which often attains a flow rate of 10 – 20 m/s. Two successive stages are often used because the collection efficiency of ejector venturi scrubbers is not much higher than that of spray towers.

Self-induced spray scrubbers (Fig. 8 C) are available in many designs. In contrast to other scrubbers, the dust-laden gas is fed through the wash fluid. The wash fluid is thus atomized, entrained, and mixed with the gas. This effect is reinforced by a redirecting vane. Entrained, dust-laden fluid collects inside the scrubber in the collection tank. The resulting slurry must be

Table 1. Operating data for scrubbers

Parameter	Packed-bed scrubber	Ejector venturi scrubber	Self-induced spray scrubber	Mechanical scrubber	Venturi scrubber
Cut size, μm*	0.7 – 1.5	0.8 – 0.9	0.6 – 0.9	0.1 – 0.5	0.05 – 0.2
Relative velocity, m/s	1	10 – 25	8 – 20	25 – 70	40 – 150
Pressure drop, kPa	0.2 – 2.5		1.5 – 2.8	0.4 – 1.0	3 – 20
Water consumption, L/m^3	0.05 – 5	5 – 20**		1 – 3**	0.5 – 5
Energy consumption, kW · h/1000 m^3	0.2 – 1.5	1.2 – 3	1 – 2	2 – 6	1.5 – 6

*Particle density $\varrho_p = 2.42$ g/cm^3.
**For each stage.

removed at intervals. Water consumption is limited to that required to replace losses associated with the gas or slurry removal.

In *rotational scrubbers* (Fig. 8 D), the washing fluid is dispersed radially in the gas by rotating spray nozzles. The gas spirals upward and exits through a tube, as in a cyclone. The dirty water is removed from the bottom of the scrubber.

The *venturi scrubbers* (Fig. 8 E) have the highest collection efficiency. The gas is accelerated to up to 150 m/s in the venturi throat (orifice). The washing fluid enters the middle of the throat just in front of its narrowest point or is fed radially into the throat. The liquid is dispersed by the inflowing gas. The dust-laden water droplets are separated from the gas in a cyclone.

Typical operating data are listed in Table 1. Increased collection (i.e., reduction in critical particle diameter) is associated with greater relative velocity and higher energy consumption. With venturi scrubbers, for example, a cut size (50 % value on the fractional efficiency curve) of about 0.1 μm can be attained, but the pressure loss increases to 20 kPa.

Scrubbers operate by transporting dust particles to the scrubbing liquor and binding them to it. The wettability of the particles does not play a crucial role in binding; wettable particles penetrate the interior of the droplet, while nonwettable particles adhere to the surface. The transport step is decisive in separation. Diffusion and condensation may certainly take place, but in general, inertial forces appear to dominate [34]. Furthermore, because the scrubbing liquor is assumed to be mostly in droplet form, the transport process can be described in clear terms.

The gas flow lines diverge as they approach the liquor droplet (Fig. 9). By virtue of their inertia, the particles follow the flow lines only partially, if at all; instead, they fly toward the droplet surface. Particles strike the droplet if their initial position in the undisturbed flow upstream of the droplet is inside a flow tube with diameter e. Particles located outside the tube bypass the droplet.

A *limiting trajectory* can thus be defined as the line separating particles that collide with the droplet from those that pass by it. The *collision efficiency* η is defined as

$$\eta = \left(\frac{e}{d_l}\right)^2 \tag{15}$$

where d_l is the droplet diameter. Observations indicate that practically all particles striking the droplet adhere to it [35]; therefore, the collision efficiency η corresponds to the single-droplet collection efficiency. Collection in the scrubber is then a result of the overall action of individual droplets. Figure 10 gives fractional efficiency curves and overall collection efficiencies for the scrubbers shown in Figure 8. Measurements were performed with sillitin, a very fine dust composed of silicon dioxide [31].

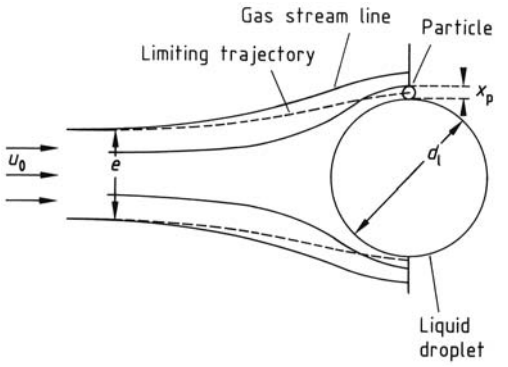

Figure 9. Trajectories and flow lines for flow past a spherical droplet
U_0 = gas velocity; e = diameter of flow tube; d_l = droplet diameter; x_p = particle diameter

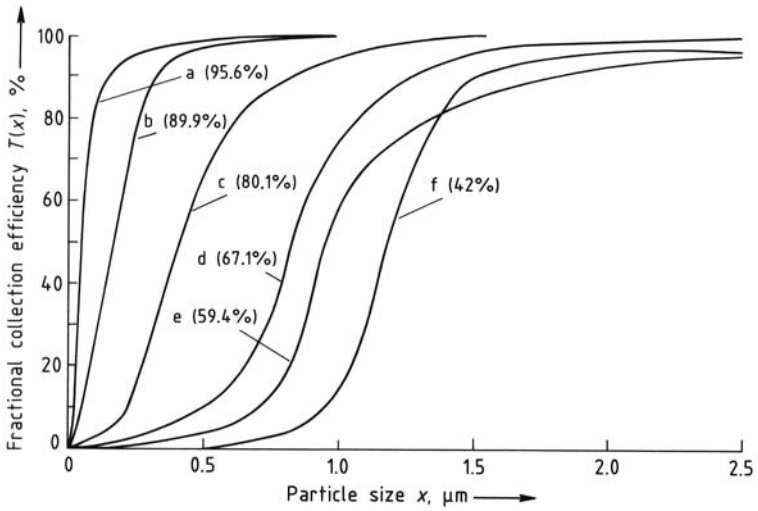

Figure 10. Fractional collection efficiencies for various scrubbers [31]
Measurements were made using sillitin, mean particle size = 1.5 µm, particle density = 2.42 g/cm^3; percentages indicate the overall collection efficiency for sillitin
a) Venturi scrubber, $\Delta p = 10$ kPa; b) Two-stage rotational scrubber; c) Single-stage rotational scrubber; d) Self-induced spray scrubber; e) Single-stage ejector venturi scrubber; f) Packed-bed spray scrubber

4.3. Design Calculations

4.3.1. Collection Efficiency

Development and sizing of scrubbers are often purely empirical because the processes that occur in these complicated pieces of equipment are complex and difficult to simulate with theoretical models. However, BARTH [36] and CALVERT [37] have proposed models that are quite helpful because (1) they allow clear identification of important parameters and trends; (2) they have been at least partly tested by experiment [5, 38]; and (3) they contain geometrical dimensions that are important for size calculations.

In these models, the scrubbing liquor is assumed to be in droplet form, and inertial forces are considered crucial in the transport of dust particles to the droplet (cf. Section 4.2). The calculation consists of three steps:

1. Calculation of single-droplet collection
2. Calculation of the gas volume cleaned by the single droplet
3. Calculation of the change in dust concentration due to the action of all droplets

The model depicted in Figure 9 is the basis for calculating the single-droplet collection efficiency; the limiting trajectory is found by solving the equations of motion for dust particles numerically. Important parameters are the Reynolds number and the Stokes parameter.

The Reynolds number *Re* for flow around the droplet is given by

$$Re = \frac{v_{rel} \cdot d_l \cdot \varrho_g}{\mu_g} \tag{16}$$

where ϱ_g is the gas density, μ_g is the viscosity of the gas, and v_{rel} is the relative velocity between the droplet and the gas.

The inertial parameter (Stokes parameter) ψ describes the dynamics of the particles:

$$\psi = \frac{\varrho_p \cdot U_0 \cdot x_p^2}{18\mu_g \cdot d_l} \tag{17}$$

where ϱ_p is particle density and x_p is particle size.

The numerical results presented in Figure 11 have been confirmed experimentally. To a good approximation [38], they can be calculated as

$$\eta = \left(\frac{\psi}{\psi + k_1}\right)^{k_2} \tag{18}$$

where η is the collision efficiency (Eq. 15) and k_1 and k_2 are constants that depend on the Reynolds number. For most operating conditions, the collection process takes place primarily in the range

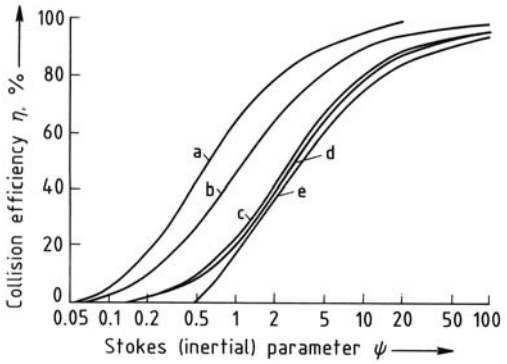

Figure 11. Calculated collision frequencies η vs. Stokes (inertial) parameter ψ for various Reynolds numbers *Re*
Values of *Re*:
a) ≫ 1, potential flow; b) 60, 80; c) 40; d) 10, 20; e) < 1, viscous flow

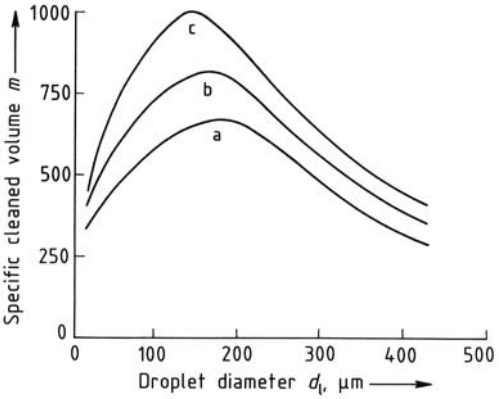

Figure 12. Specific cleaned volume vs. droplet diameter d_l for different particle sizes
Particle size x_p, µm:
a) 2.0; b) 2.5; c) 3.2
Velocity of the entering droplets w_e= 7 m/s; gas velocity U = 7 m/s

$Re < 40$. Here the results can be approximated well with $k_1 = 0.65$ and $k_2 = 3.7$ [38]. A more detailed investigation into this topic can be found in [39].

As the droplets move through the apparatus, they clean a certain volume of gas. The ratio of the cleaned volume to the droplet volume, the *specific cleaned volume m,* is the most important parameter for sizing a scrubber:

$$m = \frac{3}{2d_l}\int_{t_1}^{t_2} \eta(t) v_{rel}(t) dt \qquad (19)$$

where t is time.

The value of m is found by (numerically) solving the equation of motion (Eq. 1) for the droplet. In this way, the relative path length between the droplet and the gas in the time difference $t_2 - t_1$ (residence time) is determined.

The results depend on scrubber geometry, operating conditions (gas velocity and direction), and particle properties (size, density, initial velocity). Equation (19) thus provides an important and useful basis for sizing scrubbers. The drawback of this procedure is that the calculated results cannot be generalized but are valid only for the selected boundary conditions. Furthermore, numerical calculation requires a certain amount of computational effort, but this should not be a problem in view of the present state of computer technology.

An optimal droplet size usually exists for the specific cleaned volume, as can be seen in Figure 12. Under other operating conditions, this optimum can also occur at droplet sizes much smaller than 100 µm [5].

In the third step, the total effect of all the droplets in changing the dust concentration is calculated. The result is the fractional or overall collection efficiency.

The particle concentration c in the scrubber is expressed by

$$c = c_e \cdot \exp(-b \cdot m) \qquad (20)$$

where c_e is the particle concentration in the gas inlet to the scrubber; m is the specific cleaned volume; and b is the specific scrubbing-liquor ratio ($b = \dot{V}_l/\dot{V}_g$, where $\dot{V}_l$ is the volume flow rate of scrubbing liquor and $\dot{V}_g$ is the volume flow rate of gas). Typical b values are $(0.5 - 5)\times 10^{-3}$, i.e., 0.5 – 5 L of liquor per cubic meter of gas (see Table 1).

To find the fractional separation efficiency $T(x_p)$, m is calculated as a function of particle size x_p:

$$T(x_p) = 1 - \exp[-b \cdot m(x_p)] \qquad (21)$$

The overall collection efficiency is finally obtained by integrating the product of the fractional efficiency and the density distribution of particle size (cf. Eq. 10). The complete droplet-size distribution must be used for these calculations. If a mean, often arbitrarily selected value is used, considerable errors can occur [40].

The model proposed by CALVERT [37] utilizes the same basic approach as that of BARTH [36]. The effort required for the numerical computations is shortened substantially by fitting the equations to experimental values, so that the equation of motion for the droplets need not be solved. However, this procedure entails some loss of general applicability and information content.

For the venturi scrubber, the following equation is given:

$$T(x_p) = 1 - \exp\left[-\frac{2 \cdot \dot{V}_l \cdot d_l \cdot \varrho_l \cdot v}{55 \cdot \dot{V}_g \cdot \mu_g} F(\psi, f')\right] \quad (22)$$

where v is the maximum gas velocity, ψ is the inertial parameter (Eq. 17), and f' is an empirical fitting parameter, often in the range of 0.25 – 0.5.

The following approximation is given for the function $F(\psi, f')$ in the range $1 \leq \psi \leq 4$:

$$F(\psi, f') \approx 0.312 \cdot \psi \cdot f'^2 \quad (23)$$

Equation (22) can also be used, along with a pressure-drop equation, for optimization [5]. In general, model calculations indicate that higher relative velocities and increased addition of scrubbing liquor lead to better collection efficiency; this is also observed experimentally (Table 1).

4.3.2. Pressure Drop

Calculation of the pressure drop is of interest chiefly for venturi scrubbers. Empirical formulas and model calculations are available for this purpose.

The *empirical formulas* are based on the procedure for evaluating flow in pipes:

$$\Delta p = \xi \frac{\varrho_g}{2} v_K^2 \quad (24)$$

where v_K is the gas velocity in the venturi throat and ξ is the pressure-drop coefficient:

$$\xi = k_a + k_b \frac{\dot{V}_l}{\dot{V}_g} 10^3 \quad (25)$$

where k_a and k_b are empirical constants that depend on the equipment and thus cannot be generalized; typical values are $0 \leq k_a \leq 0.5$ and $0 < k_b \leq 1.7$.

In *model calculations,* the pressure-drop contributions of the gas and droplets are added. The droplet contribution is taken into account by solving the equation of droplet motion and by introducing the laws of two-phase flow [41]. The resulting formulas can be solved only by numerical techniques; they are in good agreement with experiment. No further details are discussed here; however, the extent of agreement between calculation and experiment depends on whether the scrubbing liquor is uniformly distributed over the total flow cross section or whether a significant fraction flows down the walls of the scrubber as a film.

Experiments have repeatedly shown that energy consumption grows as the particle cut size decreases, i.e., as collection efficiency increases. Empirical equations have also been derived on the basis of this observation [42]. Such equations are not, however, well suited to the sizing or optimization of scrubbers, because the several independent variables (equipment dimensions, dust properties, operating conditions) are not explicitly stated. The correlation between energy consumption and cut size holds only for a given size and type of equipment. Considerable discrepancies can occur between different types of scrubbers (Fig. 13) [31].

4.4. Droplet Separators

Efficient dust collection in a scrubber requires separation of the dust-laden droplets in a separator that is either integrated into the scrubber or connected downstream. Because droplet sizes generally range from 1 μm to several hundred micrometers, commercial separators utilize inertial forces to separate droplets from the gas stream. Layers of wire mesh or fabric, stacks of plates, or centrifugal devices are employed [5, 43].

Lamellar (Plate) Separators are often used because of their simple construction and low pressure drop. These devices consist of parallel channels with multiple deflections and liquid-retaining grooves (Fig. 14). The droplet-laden gas stream undergoes many changes of direction in the channels. By virtue of their inertia, droplets collide with the wall to create a film which is "peeled" off in the retaining grooves. To prevent

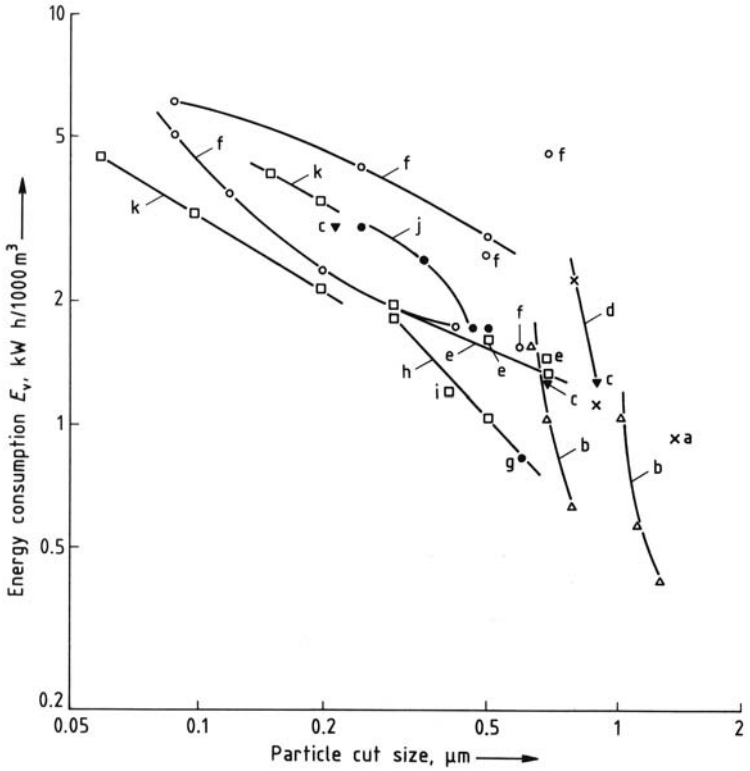

Figure 13. Energy consumption of scrubbers as a function of cut size
a) Wet cyclone; b) Spray tower; c) Self-induced spray scrubber; d) Ejector venturi scrubber; e) Low-pressure venturi scrubber; f) Rotational scrubber; g) Impinger; h) Low-pressure venturi–impinger scrubber; i) Wet cyclonette; j) Scrubber based on different principles; k) High-pressure venturi scrubber

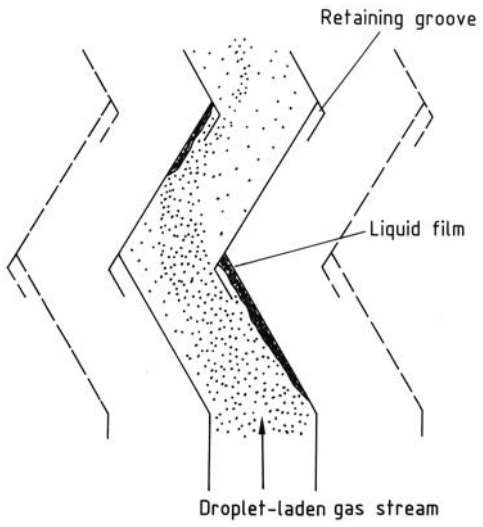

Figure 14. Droplet collection by stacks of plates

product caking, the plates can also be irrigated; a second downstream stage is then installed to trap the droplets entrained at the leading edges of the plates in the first stage. The plates can have various profiles. Typical channel widths are 20 – 30 mm; gas velocities are 5 – 10 m/s for horizontal flow and 2 – 3 m/s for vertical flow; pressure drops are a few hundred pascals. The usual cut diameters are ca. 5 – 10 µm.

Centrifugal Separators (cyclones) are often employed if high separation efficiencies are required, especially downstream of venturi scrubbers. Figure 15 shows a simple form.

Like all inertial collectors, lamellar and centrifugal separators become more efficient as flow velocity increases. However, an upper velocity limit must not be exceeded; otherwise, collected liquid is reentrained (cyclones), or the formation

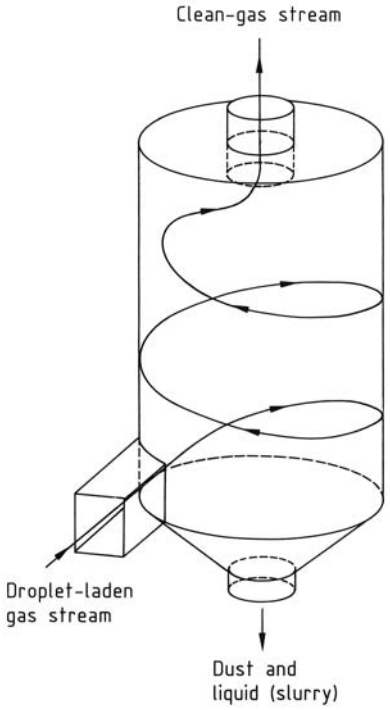

Figure 15. Centrifugal droplet separator

of secondary droplets due to impact on the liquid film becomes significant (lamellar separators). These limits must be determined empirically for each type of equipment and application.

5. Filters

5.1. General

Filters constitute an important aid in modern particle collection technology, especially when highly efficient collection in the finest particle-size range is required. Many versions are available. Of all collectors, these have the widest spectrum of applications and thus a large share of the market.

With regard to application, design, and mode of operation, filters for dust collection can be classified as deep-bed filters [44] or surface filters [45, 46].

Deep-bed Filters are used where dust loads are low, on the order of several milligrams per cubic meter of gas. Typical applications include air conditioning and ventilation, laboratory exhaust systems, clean rooms, and respiratory protection. Such filters usually consist of a relatively loose fiber mat with a pore fraction over 90 % (often > 99 %). As the gas flows through the fibrous layer, particle collection takes place in the interior of the layer where the dust accumulates (deep-bed filtration). After becoming saturated with dust, these filters are usually discarded; some can be cleaned by washing or blowing. Typical gas velocities are 0.1 – 3 m/s.

Surface Filters are used for high dust loads, on the order of several grams to hundreds of grams per cubic meter; this is the typical range for industrial dust removal and air pollution control. The filter media used to be mainly woven fabrics; today, nonwovens such as mats or needled felts, often with surface coatings, are preferred. The pore-volume fraction in these media is 70 – 90 %. Collection occurs mainly at the filter surface, in the resulting dust layer (filter cake). The dust bed is the true filter medium and is highly efficient: emission values of a few milligrams per cubic meter or less can be attained. Because the pressure drop increases as the cake grows, these filters must be cleaned periodically. Collected dust, which may be the product, is recovered. Depending on operating conditions, cleaning can take place at intervals of a few minutes to several hours. Typical gas velocities are 0.5 – 5 cm/s.

Combinations of surface and deep-bed filters have been discussed with a view to satisfying extreme emission limits (e.g., 0.1 mg/m^3).

Because filter design and functioning as well as system design differ greatly for deep-bed and surface filters on the one hand, and those using fibrous layers and granules on the other, three groups are discussed separately.

5.2. Fibrous Filters (Deep-Bed Filters)

5.2.1. Mode of Operation and Basic Designs

The fibrous layers in filter-medium systems consist mainly of synthetic fibers (glass or polymers). Table 2 summarizes typical geometrical data. The spacing between the fibers is large compared with the size of the particles to be

Table 2. Geometrical data for deep-bed filters

Parameter	Coarse filter	Submicrometer filter
Fiber diameter D_F, μm	50 – 100	1 – 5
Mat thickness Z, cm	1 – 3	0.1 – 0.3
Fiber volume fraction $(1 - \varepsilon)$, %	< 1	< 5 – 10
Mean fiber spacing	9 D_F	3 D_F

collected. This implies that the filters do not function as a sieve; the purely geometrical blocking action is not crucial for particle collection. Various mechanisms (diffusion, inertia, electrostatic attraction) cause the particles to be transported to the fibers, where they must then adhere.

Filter mats are installed in a variety of ways in accordance with plant requirements and available space. Figure 16 shows the most important types. In the simplest case (A), the flat filter mat is inserted perpendicular to the direction of flow. To increase filtration area (lower flow velocity → lower pressure drop → longer lifetime for a given channel cross section), the filter is often folded and mounted in a frame. A further gain in filtration area is obtained by a zigzag placement of frames with folded filter mats (B).

Because the filters become plugged with collected dust over time, they must be replaced at certain intervals (usually several months to years). The method used for filter mounting is therefore very important. The mount must be tight but easy to handle. Filter replacement can be effected, for example, with a roll filter arrangement (C). This rather costly design has been increasingly superseded by stationary zigzag filters (B) or by pocket filters (D). This avoids the danger of releasing collected dust when the filter strip is advanced.

The main application for fibrous deep-bed filters is inlet-air cleaning, i.e., for low dust loads. However, since the early 1980s high-efficiency filters have been used in exhaust-gas systems where particle loads are higher but the clean gas must have especially low particle concentration, e.g., for toxic or harmful dusts composed of

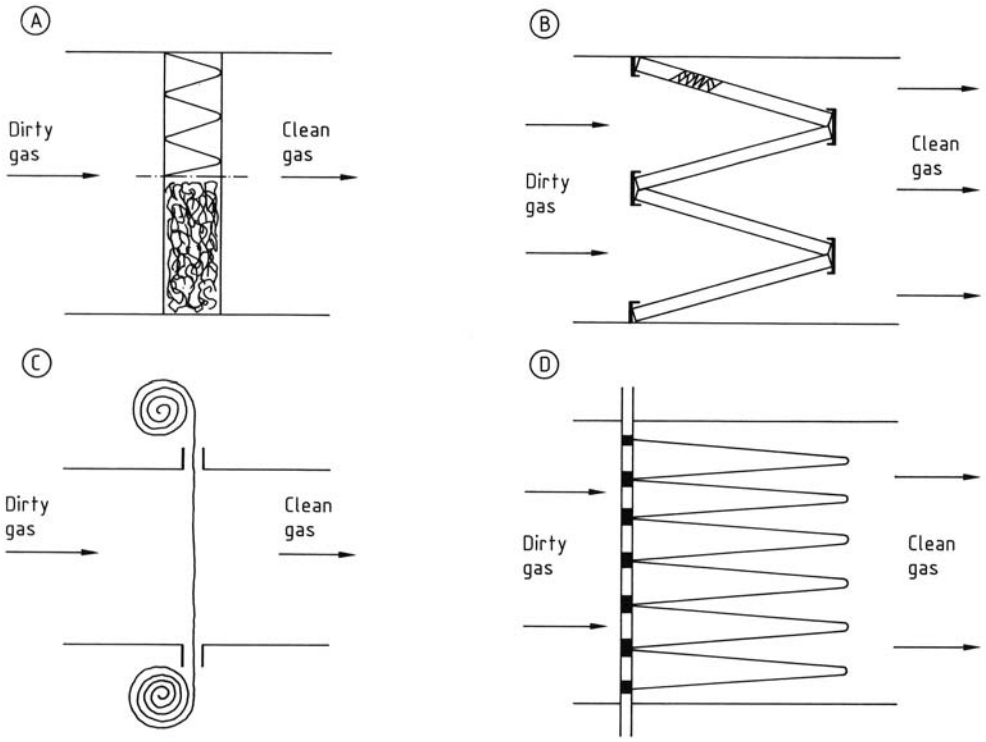

Figure 16. Designs of fibrous deep-bed filters A) Flat filter; B) Stationary zigzag filter; C) Roll filter; D) Pocket filter

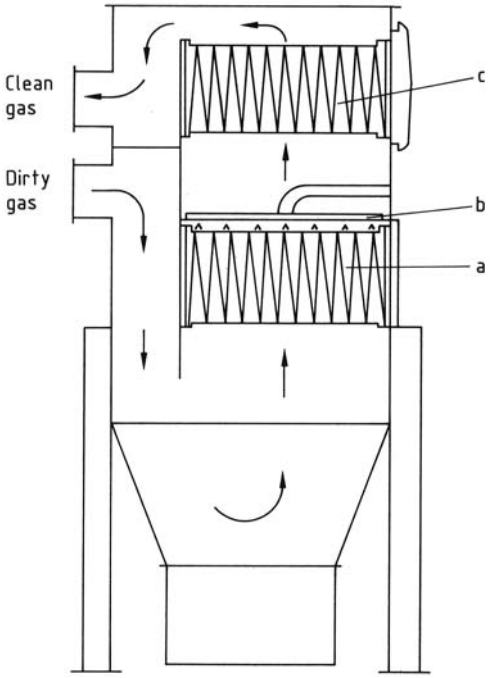

Figure 17. Exhaust-gas cleaning system employing submicrometer filters
a) First filter stage; b) Nozzle carriage for cleaning filter; c) Second filter stage

heavy metals or radioactive substances. Two-stage submicrometer filters are then used (Fig. 17). The first stage (a) is periodically cleaned by reverse blowing with a reciprocating nozzle carriage (b). The second stage (c) is replaced after it is saturated with dust; because of the low dust concentration, replacement intervals are sufficiently long. The usual cleaning procedure for such a system involves shutting off the gas stream, so for continuous operation at least two units must be connected in parallel. Development work aimed at finding application limits, optimal designs, materials, and operating conditions is still under way. Problems must be expected for very fine, highly adhesive dust, or if the folds in the first filter stage are too narrow. The collection efficiency for such a system may be very good; emission values of 0.1 mg/m^3 or less can be achieved even with a dirty-gas dust load of 10 g/m^3 or more.

The range of collection efficiencies for deep-bed filters varies widely and depends on the design and operating conditions. It extends from a single prefilter for relatively coarse dust to submicrometer particulate filters for clean rooms, where the DIN-EN standard requires a collection efficiency of up to 99.999995 % for the most penetrating particles [most penetrating particle size (MPPS) $\approx$ 0.1 – 0.4 µm] [47].

With regard to temperature, deep-bed filters are used mainly at < 100 °C. In paint shops, temperature resistance up to 120 °C is required. Some designs can also be used up to 300 °C. These filters generally employ glass fibers in metal cartridges with appropriately temperature-resistant sealing materials.

Another application of deep-bed filters is the collection of liquid droplets, especially oil or acid mist. Here, the collected liquid flows continuously downward out of the filter, so that the pressure drop is stable. A variant of this use is the collection of soluble dusts with simultaneous solvent feed. Again, the collected material flows continuously out of the filter layer.

5.2.2. Design Calculations

The models for calculation presented in this section refer to unloaded filters, i.e., to the initial conditions. With regard to collection efficiency, this is usually the critical state because collection generally improves with increasing dust load (electret filters are an exception). The methods proposed in the literature for calculating filtration behavior over time are not discussed because they are very complex and still of limited practical use [48].

5.2.2.1. Collection Efficiency

The fractional collection efficiency $T(x)$ of a fibrous layer is given by

$$T(x) = 1 - \exp[-f' \cdot \varphi(x)] \tag{26}$$

For fibers of circular cross section,

$$f' = \frac{4}{\pi} \cdot \frac{1-\varepsilon}{\varepsilon} \cdot \frac{Z}{D_F} \tag{27a}$$

$$f' = \frac{4}{\pi} \cdot \frac{1}{\varepsilon} \cdot \frac{M}{D_F \cdot \varrho_F} \tag{27b}$$

$$f = f' \cdot \varepsilon \tag{27c}$$

where ε is the porosity, Z is mat thickness, D_F is fiber diameter, M is filter mass per unit filter area, and ϱ_F is the fiber density.

The geometric factor f represents the ratio of the projected fiber area to the filter face area. For prefilters $f \approx 3 - 10$; for high-efficiency submicrometer filters, $f \approx 100 - 300$.

The factor φ (x) is the collection efficiency of a single fiber inside the mat. Because collection in a medium (depth) filter includes transport and adhesion of the particles to the fiber,

$$\varphi = \eta \cdot h \tag{28}$$

where η is the collision efficiency and h is the adhering fraction. This factor is included because at the usual filtration velocities and especially for particle sizes > 1 μm, not all the particles hitting the fiber surface for the first time adhere [49, 50].

Since the 1930s, research has been concerned with determining η. The importance of the adhering fraction h was not recognized until the 1960s, but research on this factor has been increasing.

Particles can be transported to the fiber surface in three ways: Brownian diffusion, inertial forces, and electrostatic interaction (Fig. 18).

1. *Brownian Diffusion.* The random motion of particles about their mean trajectory [Fig. 18 (a)] is due to the thermal motion of gas molecules (Brownian motion); it can be calculated with Fick's diffusion equations. For engineering purposes, this effect is important chiefly for particles smaller than ca. 0.5 μm and velocities lower than 10 cm/s. This diffusion effect η_D is governed by the following relation:

$$\eta_D \sim \left(U_0 \cdot D_F \cdot x \cdot \frac{\mu_g}{T} \right)^{-2/3} \tag{29}$$

where U_0 is the velocity of the incident gas stream, μ_g is the viscosity of the gas, and T is the absolute temperature.

2. *Inertial forces* [Fig. 18 (b)] cause a predetermined movement of particles toward the fiber. These processes can be described by the equation of motion (Eq. 1).
The decisive parameter for the inertial effect is the inertial (Stokes) parameter

$$\psi = \frac{\varrho_p \cdot x^2 \cdot U_0}{18 \cdot \mu_g \cdot D_F} \tag{30}$$

Inertial effects are important mainly for particles larger than 0.5 – 1 μm. As ψ increases, the collision efficiency number rises rapidly. The Reynolds number for flow past the fiber is also important because the collision efficiency number increases with the Reynolds number.

3. *Electrostatic interactions* [Fig. 18 (c)] can also be described by the equation of motion.

Figure 19 presents measurements of the fractional collection efficiency of a fibrous layer [51].

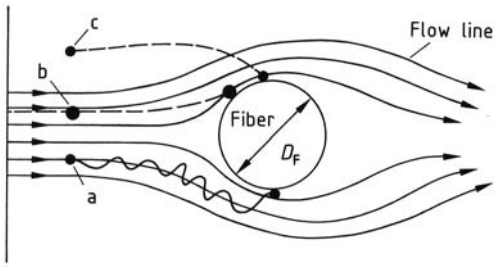

Figure 18. Transport mechanisms for particle collection on fibers
a) Brownian diffusion; b) Inertial forces; c) Electrostatic interaction

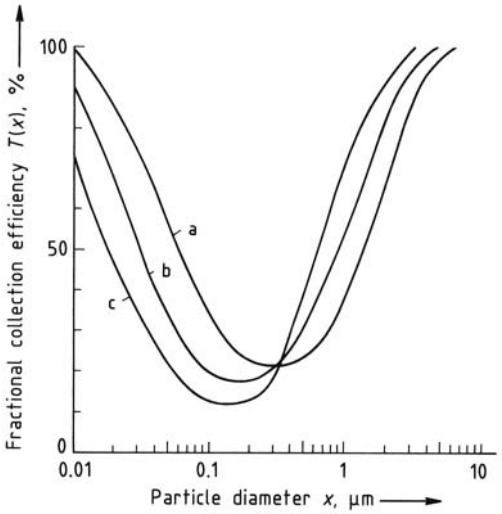

Figure 19. Fractional efficiency curves for a glass-fiber filter at various superficial velocities
Superficial velocity U_0, m/s:
a) 0.055; b) 0.2; c) 0.5
Values for $x > 0.5$ μm were determined with a quartz aerosol and for $x < 0.2$ μm with a sodium chloride aerosol

Characteristic influences of the diffusion and inertial effects can be seen at particle diameters < 0.1 and > 0.5 μm, respectively. In the transition region (ca. 0.1 – 0.5 μm), both effects are very slight. This minimum in the fractional efficiency curve is typical; it represents the critical particle-size range for the filter. For this reason, filter tests are often performed with particle sizes ca. 0.3 μm.

One way of overcoming the efficiency minimum is to utilize electrostatic interactions [Fig. 18 (c)]. Electrostatic forces act over long ranges and can thus attract particles from the flow even if they are far from the fiber.

Calculation of electrostatic effects is very complicated because many configurations of charges and fields are possible. "Electret" filters have attracted much interest. These devices consist of fibers on which a charge is imposed during manufacture [52]. The charge is localized not at the fiber surface but in its interior. Such fibers greatly improve collection, even of uncharged particles (Fig. 20). If the particles carry only a small charge (e.g., are in equilibrium with the ion concentration in air), even the size range below 0.1 μm is collected quite efficiently [Fig. 20, curve a]. The advantage of the electret filter is that, with comparatively slight pressure drops, the collection efficiency is much higher than that of conventional filters, especially in the critical transition region. Its drawback is that its behavior deteriorates with time because, as more particles are deposited on the fibers, the electrostatic effects weaken (depending on particle properties). Further experimental and theoretical results can be found in [51].

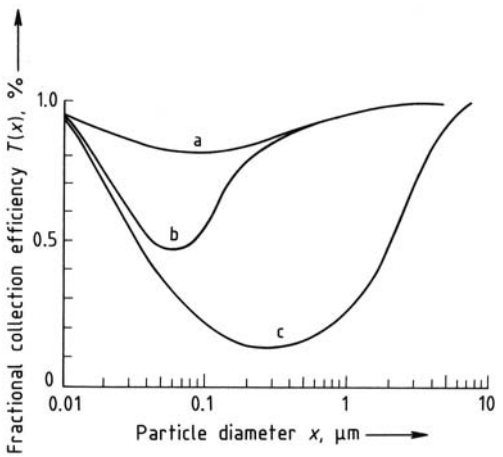

Figure 20. Fractional efficiency curves for an electret filter spun from a polymer solution
a) Fibers and particles charged; b) Fibers charged, particles uncharged; c) Fibers and particles uncharged. Superficial velocity $U_0 = 0.1$ m/s

To obtain the single-fiber collection efficiency φ from the transport parameter η, information is needed about the adhering fraction h (Eq. 28); this is important not only for single fibers but also for fibrous beds. Extensive studies have shown that the adhering fraction generally depends on flow velocity, fiber geometry, particle geometry (size and shape), and surface properties of the fiber and particle [50]. Bouncing of particles from the fibers can begin at velocities lower than 10 cm/s. As the velocity and particle size increase, the adhering fraction usually decreases. Therefore, adhesion in the particle-size range > 1 μm should always be given special attention.

Besides bouncing, resuspension of already collected particles can cause severe problems. The concentration of bio-aerosols, for example, can reach higher values in the "clean gas" than in the original raw gas [53].

The fiber configuration in the filter layer is another aspect that was formerly neglected. Theoretical calculations usually assume a homogeneous distribution of fibers; this is certainly not the case, and uneven distribution strongly affects the collection efficiency. As the inhomogeneity increases, collection usually becomes poorer. More detailed information is given in [54–56].

5.2.2.2. Pressure Drop

The pressure drop generated in flow through a filter medium can be described by the "drag" model. The pressure drop is attributed to the drag involved in flow past the fibers; in view of the low volume fraction of fibers ($< 5\,\%$), this is certainly realistic in physical terms.

Accordingly,

$$\frac{\Delta p}{Z} = \frac{2}{\pi} \cdot \frac{\varrho_g \cdot U_0^2}{D_F} \cdot \frac{(1-\varepsilon)}{\varepsilon^2} \cdot C_D(Re) \qquad (31)$$

where Z is the thickness of the fiber layer, ε is the porosity of the fiber layer, and U_0 is the incident flow rate. The drag coefficient C_D depends on the Reynolds number for flow past the fibers:

$$Re < 1: \quad C_D = \frac{8\pi}{Re(2-\ln Re)} \tag{32a}$$

$$1 \le Re \le 50: \quad C_D \approx \frac{10}{Re} + 1.5 \tag{32b}$$

where

$$Re = \frac{U_0 \cdot D_F \cdot \varrho_g}{\mu_g \cdot \varepsilon} \tag{32c}$$

Essential assumptions for derivation of these equations are that the fibers are circular–cylindrical and homogeneously distributed and that the incident flow is perpendicular to the fiber axes. Furthermore, the equations hold only for the initial filtration state, i.e., with no dust on the filter. Within these constraints, agreement with experiment is good. For practical purposes, however, time-dependent behavior is often more important, i.e., the dependence of pressure drop on the quantity of dust trapped. However, because no reliable way of calculating this relationship is known, the time dependence must be determined by experiment. Optimization can be based on the pressure-drop equation (Eq. 31) and the efficiency equation (Eq. 26) [5] and can give useful information on the design of medium filters.

5.3. Fabric Filters (Surface Filters)

Surface filters are used widely because of their excellent collection performance, even for the finest particles; their adaptability to the most diverse conditions; and significant advances in the development of new filter media (e.g., improved chemical resistance, heat resistance, and cleaning properties). Cake filters are available with filtration areas from a few to several hundred thousand square meters. For a properly designed, well-maintained filter, emission values can be held to a few milligrams per cubic meter (in the best cases less than 1 mg/m^3). The allowable temperature range extends to ca. 250 °C for PTFE and glass-fiber filters. Special metal fibers permit operation up to ca. 600 °C; sintered silicon carbide and other ceramic filters can function to 1000 °C, but they cost substantially more. Filtration rates are typically 40 – 180 m^3 h^{-1} m^{-2} and reach 300 m^3 h^{-1} m^{-2} in exceptional cases; typical pressure drops are 1 – 3 kPa.

5.3.1. Mode of Operation

The principal surface-filter media are nonwovens and (needled) felts that are composed of randomly arranged glass, plastic, or ceramic fibers. Woven materials, chiefly constructed from glass-fiber yarns or metal wires, are also employed.

Only at the beginning of filtration do these media trap particles in the interior of the fibrous layer. As more dust is deposited, it bridges the fibers and forms a dust layer (filter cake) on the surface.

Figure 21 shows a typical example of filtration behavior for a needled felt, in which the initial emission value was 66.5 mg/m^3 and decreased to 2.3 mg/m^3 after 46.8 g/m^2 of dust had been deposited.

The fractional efficiency curves in Figure 22 clearly show the improvement in collection performance as more dust is collected. The new, clean filter gives a typical depth-filter curve (a); after 5 min, the efficiency is over 99 % throughout the particle-size range covered (f). Since the cake-formation phase lasts only a short time for the dust loads usually encountered in practice, the interception effect inside the cake is dominant. This process is called surface filtration.

As the amount of dust deposited in and on the filter grows, the pressure drop also increases. After a certain time, or when a predetermined pressure-drop value is reached, the dust must be removed (cleaned off) to regenerate the filter. Filtration periods may be 10 min or less when the amount of incident dust is large (i.e., high concentration and high velocity); if the dust load is small, filtration can last several hours. As a rule, filters should be regenerated only when absolutely necessary (cf. Section 5.3.2); this saves operating costs and reduces emissions.

In modern commercial filter media, surface coating or treatment is used to attempt collection on the surface right from the start and to prevent particles from penetrating into the medium. This approach yields high initial collection efficiencies, avoids the danger of plugging, and facilitates removal of the filter cake.

5.3.2. Basic Designs

The three most important basic surface-filter designs are round bag, envelope, and cartridge

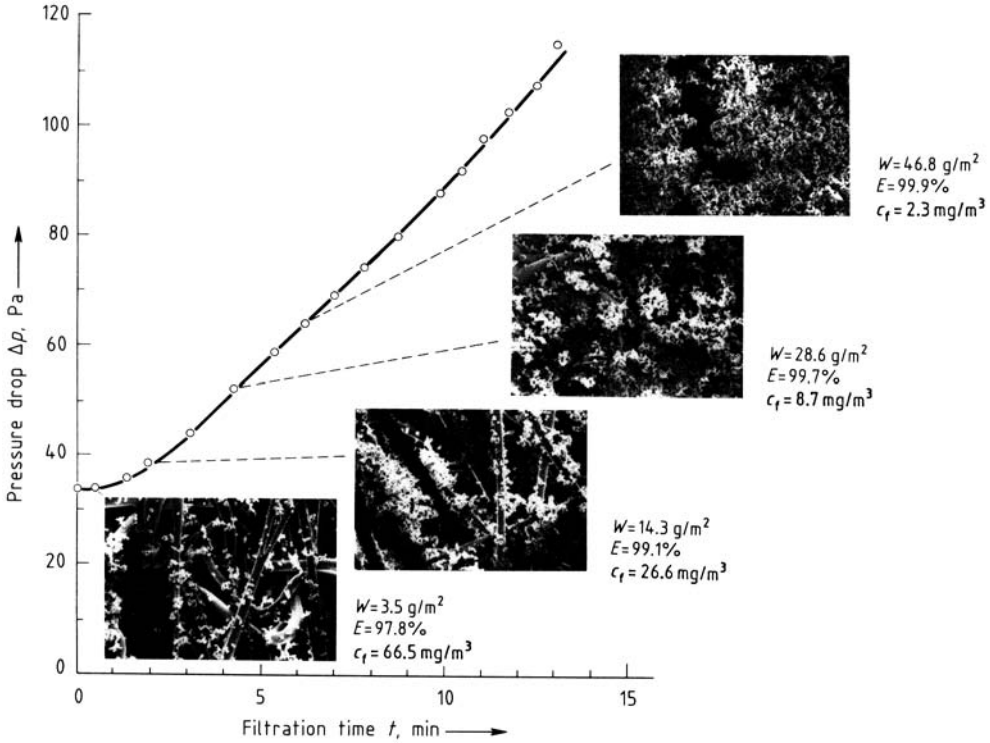

Figure 21. Time dependence of filter-cake formation, pressure drop, and dust collection on a needled felt
W = amount of dust deposited; E = total collection efficiency; c_f = dust content of clean gas; dust content of dirty gas = 3 g/m^3; gas face velocity = 150 m/h

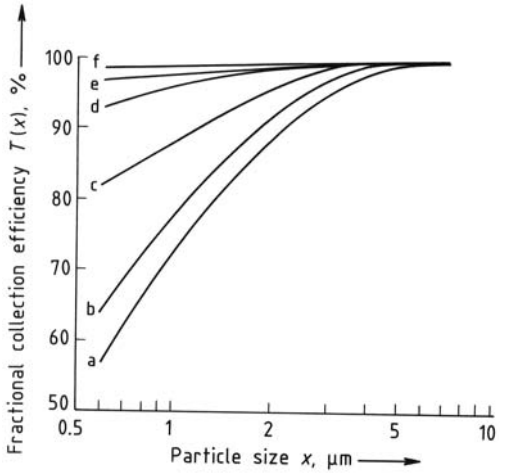

Figure 22. Variation in fractional collection efficiency due to dust deposition on a polyester needled felt
Amount of dust deposited, g/m^2:
a) 4, Δp = 33 Pa; b) 14; c) 29; d) 47; e) 75; f) 95, Δp = 110 Pa
Dust content of dirty gas = 3 g/m^3; gas face velocity = 150 m/h

(Fig. 23) if flexible media are used. Similar shapes can be realized with rigid media made, for example, from sintered plastic grains. A filter unit contains the requisite number of filter elements connected in parallel. Designs differ primarily in the method of cleaning and sometimes in the way the dirty gas is introduced [46, 57, 58].

Round (Tubular) Bag Filters are used most widely. If gas flow during filtration is inward, as shown in Figure 23 A, a retainer (supporting cage) is required. Sometimes, however, flow is outward and, in this case, only a few stiffening rings need be incorporated in the bag. Typical bags are 100 – 300 mm in diameter and 1.5 –10 m long. The filtration area per bag can thus be as much as 10 m^2.

The classical design, introduced in 1887 by the Beth company, is a *multichamber filter with shaker cleaning* (Fig. 24). Dirty gas is fed into the bags from below; it then flows through the filter medium (f) and is led to a clean-gas duct (d)

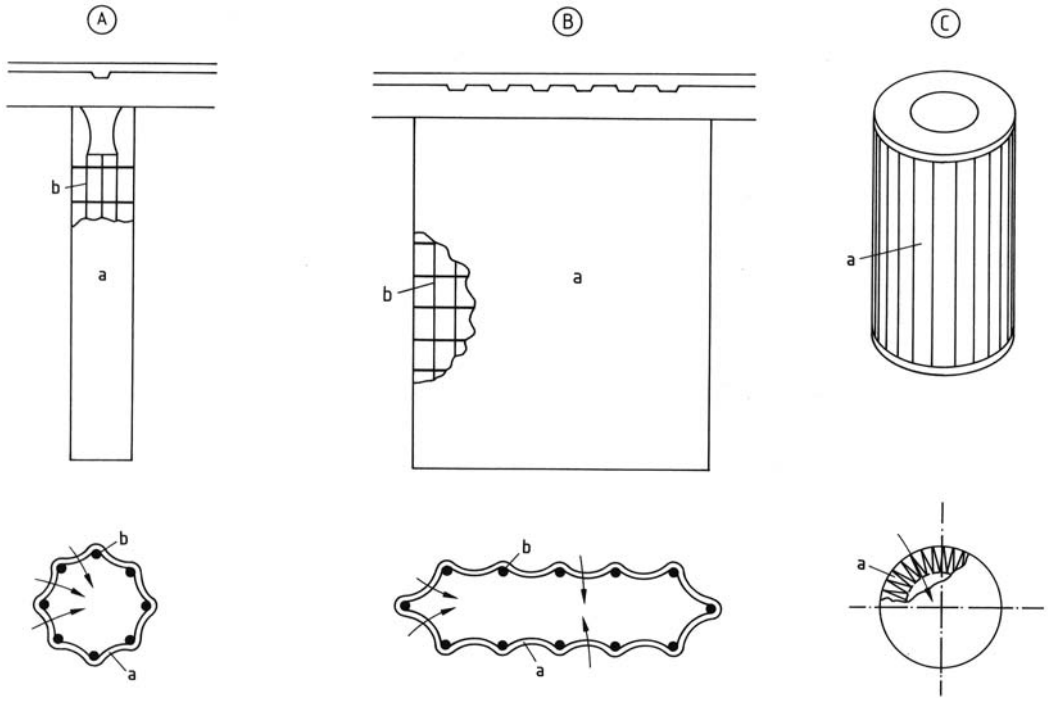

Figure 23. Basic filter designs
A) Round bag filter; B) Envelope filter; C) Cartridge filter
a) Flexible filter medium; b) Supporting cage

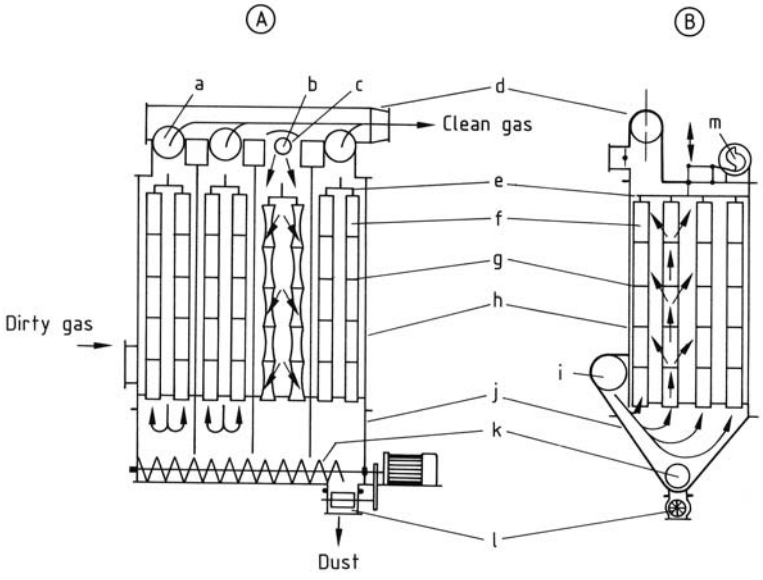

Figure 24. Multichamber bag filtration plant with shaker cleaning
The two vertical sections (A) and (B) are at right angles to each other
a) Valve open for filtration; b) Valve closed for cleaning; c) Purge air inlet; d) Clean-gas duct; e) Bag support; f) Filter bag; g) Stiffening ring; h) Filter housing; i) Dirty-gas duct; j) Dust hopper; k) Screw conveyor; l) Air lock; m) Shaker mechanism

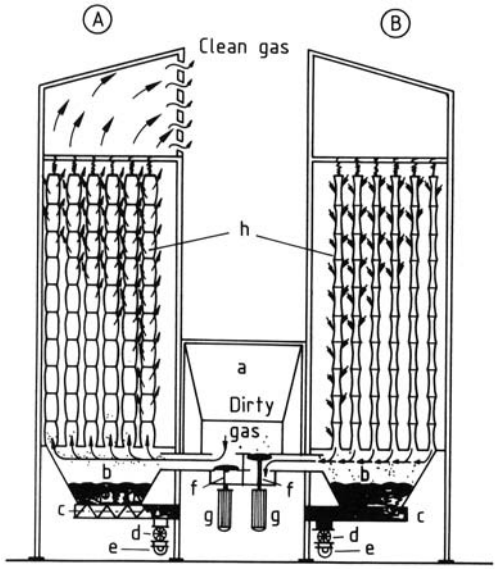

Figure 25. Baghouse with low-pressure reverse flushing
A) Operating filter chamber; B) Filter chamber being cleaned
a) Dirty-gas pressure duct; b) Dust hopper; c) Hopper screw conveyor; d) Air lock; e) Screw conveyor; f) Flushing gas duct; g) Cleaning valve; h) Filter bag

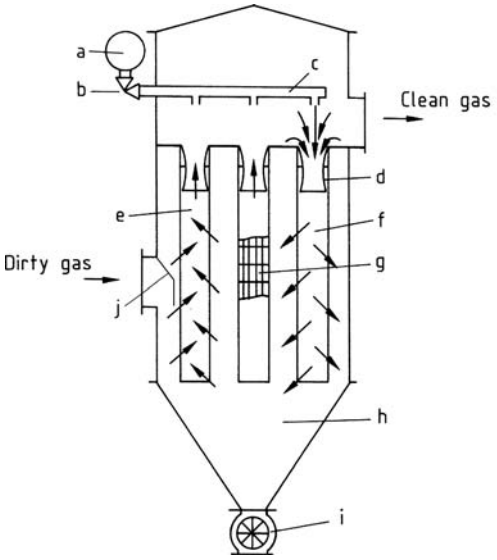

Figure 26. Round bag filter with reverse-pulse cleaning
a) Compressed-air tank; b) Right-angle diaphragm valve; c) Compressed-air duct with nozzles; d) Venturi nozzle; e) Filter bag in operation; f) Filter bag being cleaned; g) Retainer; h) Dust hopper; i) Air lock; j) Deflecting shield

at the top of the device. Particle collection takes place on the inside of the bags. For cleaning, the dirty-gas supply is cut off from one chamber at a time, and the dust is loosened by shaking or rapping the bag support. The dust removed from the bags falls into a dust hopper; purge air drawn into the bags from outside aids this process. Because the bags being cleaned are cut off from the gas flow, several filter chambers must always be used in parallel.

Large multichamber filtration plants (e.g., for cleaning flue gas from furnaces or use in the cement and metallurgical industries [45]) are often designed as *baghouses* (Fig. 25). The bags are usually large (300 mm in diameter, 10 m long). The dirty gas flows from the inside to the outside of the bags, which are cleaned by low-pressure reverse flushing (Fig. 25 B). The reversal of flow for cleaning causes the bags to collapse and the dust to drop out. In connection with the surface-coated filters mentioned in Section 5.3.1, this design offers a particularly economical approach.

Pulse-jet filters (bag filters with reverse-pulse cleaning) became more widely used as progress was made in needle felts. This design dominates in small and intermediate-size units. The gas always flows from outside to inside (Fig. 26), so the bags must be pulled over supporting cages. For cleaning, a jet of compressed air is admitted to the bag through its open top end. The pressure needed in the air tank depends on the design (0.3 – 0.7 MPa). The compressed-air jet suddenly raises the pressure in the bag, which is rapidly inflated and gas flow is reversed. The dust is thus dislodged from the outside of the bag; the process lasts ca. 0.1 – 0.3 s. Because single bags or single rows of bags must be removed from the filtration process for only a short time, the filter does not have to be divided into chambers. Cleaning is done on-line; however, off-line cleaning, in which the dirty-gas flow is cut off in a multichamber filter, may be preferable in extreme cases, e.g., for very fine dusts. Further details on the design and properties of pulse-jet filters can be found in [45, 46, 57].

Envelope Filters (Fig. 23 B) are not as widely employed as round bag filters. They are used mainly to remove dust from small amounts of gas, e.g., in silo venting, and as bunker top filters [57].

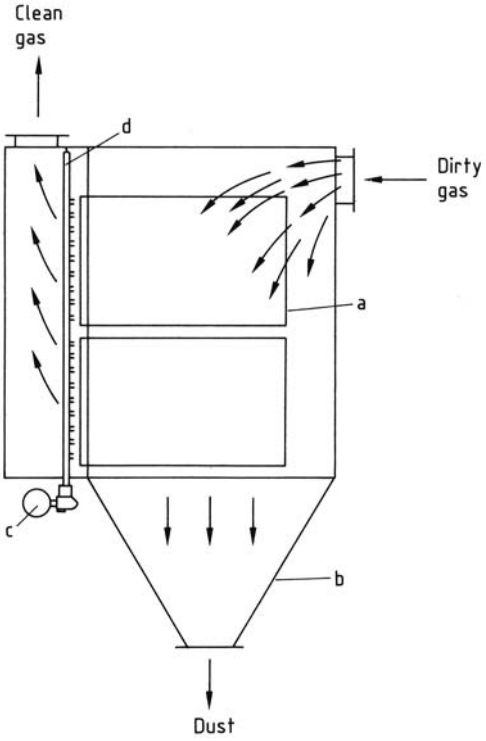

Figure 27. Schematic of an envelope filter unit with reverse-pulse cleaning
a) Envelope filter; b) Dust hopper; c) Compressed-air tank; d) Compressed-air duct with nozzles

Flow is always from outside to inside. The filter medium is stretched over a flat, rectangular, supporting cage; dust is collected on the outer surface of the medium. Envelope filters are usually smaller than round bags; filtration areas are often 0.1 – 1.5 m^2. An envelope filtration unit is shown in Figure 27. The usual cleaning method is intermediate-pressure reverse flushing or reverse pulsing. As a rule, multichamber design is not necessary.

Cartridge Filters are a further development in surface filters. The filter medium is folded in star fashion (Fig. 23 C) to pack more filtration area into a unit volume. With a standard cartridge height of 606 mm, the filtration area is between 5 and 20 m^2, depending on the depth and angle of the folds. Gas flow is always from outside to inside. A multichamber cartridge filter unit is shown in Figure 28.

The filter cake on the outside of the filter is removed either by cutting off the dirty-gas stream and flushing at low pressure with circulating nozzles (multichamber design) or by applying a reverse pulse (on-line). Cartridge filters are very compact devices that offer a relatively large filtration area in the enclosed volume. As a result, low filtration velocities are possible; this is an advantage with respect to emission levels and costs. Until now, however, cartridge filters have been useful only for easily removable dust; their development continues.

5.3.3. Operating Characteristics

Particle collection in a surface filter occurs mainly in the dust layer formed on the surface (Section 5.3.1); efficiencies greater than 99.9 % are possible independent of particle size. Therefore, this highly efficient cake must be retained on the surface as long as possible.

Figure 29 A shows that the pressure drop Δp increases as more dust is deposited, and periodic cleaning is necessary. After cleaning, the pressure drop falls to a value Δp_1 that depends on the flow resistance of the filter medium (including residual dust not removed); Δp_1 is higher than the initial pressure drop Δp_0 of the new, clean filter. For stable filter operation, Δp_1 must reach an approximately constant value after an induction period that can last several days to weeks. The filter medium, filtration velocity, and the method and intensity of cleaning determine whether stable filtration is attained for given gas and dust properties.

During and immediately after cleaning, the particle content of the clean gas increases (Fig. 29 B). This occurs partly because the filter cake, which acts as a layer of filter aid, has been removed and must be rebuilt. Especially with reverse-pulse cleaning, some of the dust passes through the filter medium because after the pressure pulse inside the bag has decayed, the filter medium falls back against the retainer and knocks part of the dust through the filter (seepage effect).

Many laboratory and plant studies have shown that the peak concentrations after cleaning may be crucial for the emission value [5, 59]. The maintenance of low emission levels thus demands that cleaning be done as seldom and as carefully as possible. Accordingly, filtration velocities should not be too high, and pressure

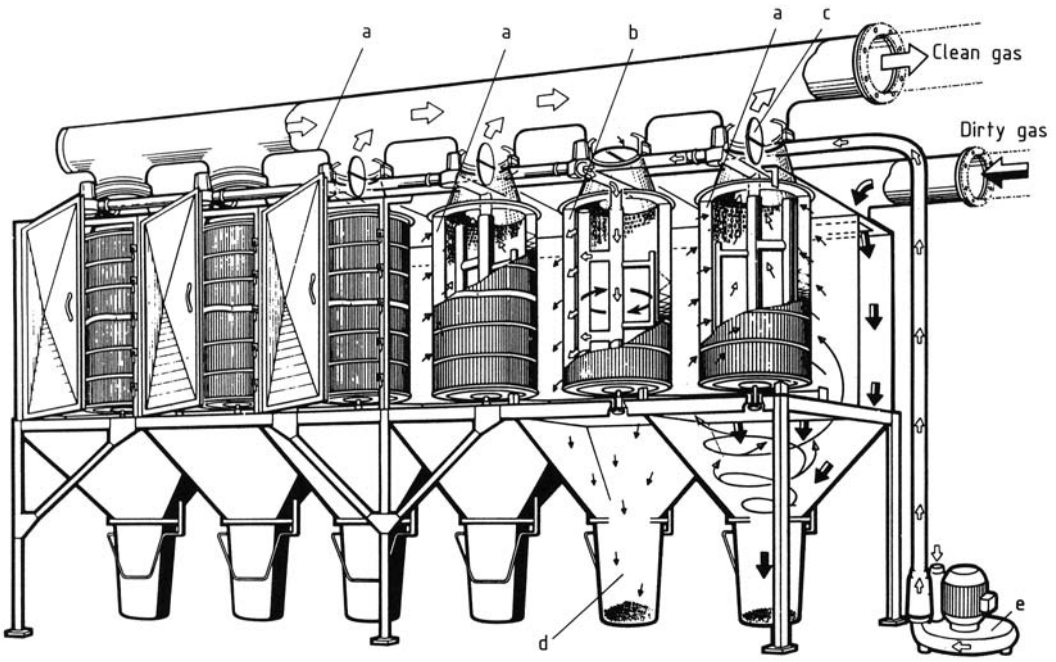

Figure 28. Multichamber filtration unit (Mann & Hummel)
a) Filter in operation (valve open, dust collects on the outside of the filter); b) Filter cleaning (valve closed, cleaning air is pumped outward through the filter and dust falls into the hopper); c) Valve; d) Dust hopper; e) Pump for cleaning air

drop – rather than time – should be used as a criterion for cleaning.

Influencing the operational behavior of surface filters by raw-gas conditioning (dosing of additives and precoating) and other techniques (e.g., electrostatic and acoustic methods) is described in [60]. In some cases considerable potential for improvement exists with regard to pressure drop, filter-medium regenerability, and particle emissions. At present, however, these methods can not be regarded as the industrial state of the art.

5.3.4. Design Calculations

The main purpose of surface-filter design is to determine the required filtration area *F,* which is given by

$$F = \frac{\dot{V}}{v} \tag{33}$$

where $\dot{V}$ is the volume flow rate of dirty gas and v is the filtration velocity; v, the ratio of flow rate to filtration area, is often called the *air to cloth ratio* and is expressed in $m^3\ h^{-1}\ m^{-2}$ or m/min. A proper selection of filter load determines the pressure drop and, ultimately, the emission value.

The filtration velocity is selected on the basis of empirical values because of a lack of generally valid theoretical models. The VDI 3677 standard gives guideline values [58]. A base load value can also be employed, which is modified for actual conditions by means of various correction factors [57].

$$v = v_0 \cdot c_1 \cdot c_2 \cdot \ldots \cdot c_n \tag{34}$$

where v is the effective filtration velocity, v_0 is the base value, and $c_1 - c_n$ are correction factors. This method is used chiefly for filters with reverse-pulse cleaning. The correction factors always refer to a defined table of base values. They differ from one author to another, being purely empirical and specific in nature.

In describing the time dependence of the pressure drop (Fig. 29), Δp is assumed to be the sum of the contributions of the medium (Δp_1) and the filter cake (Δp_2):

$$\Delta p = \Delta p_1 + \Delta p_2 \tag{35}$$

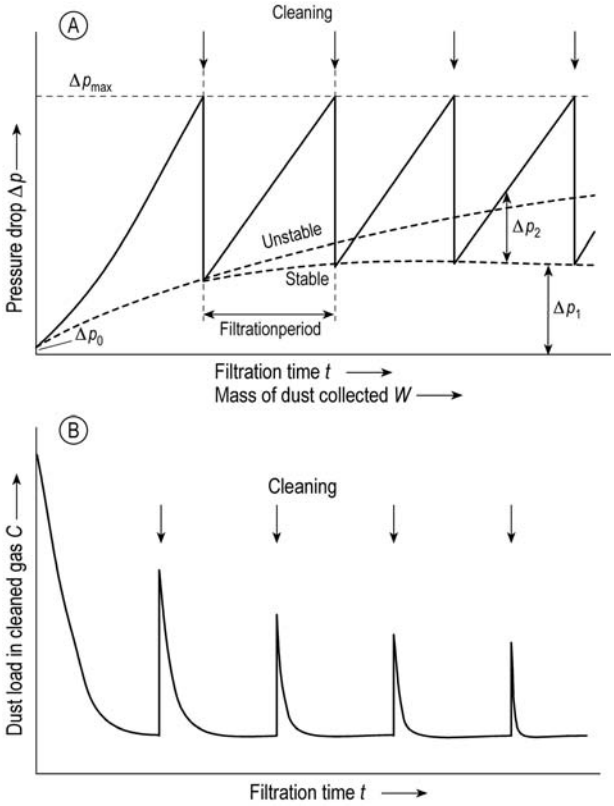

Figure 29. Pressure drop (A) and dust content (B) in clean gas vs. filtration time or mass of dust collected at constant filtration velocity
The values Δp_1 and Δp_2 denote the pressure-drop contributions of the filtration medium and filter cake, respectively

Because flow through the filter takes place at low Reynolds numbers (< 1), Darcy's law is also assumed to hold:

$$\Delta p = K_1 \cdot \mu_g \cdot v + K_2 \cdot \mu_g \cdot W \cdot v \quad (36)$$

where K_1 is the residual resistance of the filter medium after cleaning, K_2 is the specific resistance of the filter cake, W is the mass of dust collected per unit filter area, and μ_g is the viscosity of the gas. Since W is proportional to filtration time, the second term in Equation (36) increases with time and describes the time dependence of Δp.

Important parameters in Equation (36) are the resistances K_1 and K_2; as a rule, they are not constants but functions of several variables. Prediction of these parameters is still problematic because the functions are not known well enough [5, 57]. Even when K_1 and K_2 can be determined by experiment, great care must be taken to ensure that conditions in the experimental device and the full-scale plant are comparable.

5.4. Granular-Bed Filters

5.4.1. General

In granular-bed filters, the dust-laden gas stream flows through the bed and is thereby cleaned. The granular bed functions as a filter medium and in most cases can be considered a depth or deep-bed. Under some conditions, however, dust bridges and then a filter cake are formed, so that surface filtration can occur.

Besides pure particle collection, the removal of gaseous components in granular-bed filters ("dry sorption" of gases such as sulfur dioxide, hydrogen chloride, and hydrogen fluoride) has attracted increasing interest (→ Adsorption).

Granules for these applications must be made of appropriate sorbents (often calcium compounds). As a result of more stringent demands for air pollution control, the combined collection of dust and noxious gases may become still more important for small and medium-sized installations. However, only particle collection is discussed here.

The applications of granular-bed filters are determined by the material properties of the granules making up the bed. Examples of such materials are gravel, sand, ceramics, and activated carbon.

Granular-bed filters are used chiefly for the removal of hot, chemically aggressive, abrasive, or adhesive dust or when danger of fire exists. Main applications are in the lime and cement, rock and soil, metallurgical, chemical, and nuclear industries.

The service temperature range is limited by the materials used for plant construction rather than by the filter granules; in some cases, the behavior of the collected particles is also important. Operation up to 450 °C presents no problem; with special designs, 800 °C or more is attainable.

5.4.2. Mode of Operation

Granular beds can be either fixed or moving. Table 3 presents typical operating data.

Fixed-bed granular filters are operated batchwise; i.e., when dust deposition has raised the pressure drop to a predetermined limit, the dirty-gas stream is cut off and the bed is regenerated in one of two ways. Either the dust is removed internally by reverse flushing and agitation or stirring, or else it is removed externally by screening or other means. For continuous operation, these techniques always require several chambers in parallel, which are regenerated in rotation.

Table 3. Typical data for granular-bed filters

Parameter	Value
Granule diameter, mm	0.5 – 5
Bed heights, cm	5 – 20
Porosity, %	40 – 50
Incident flow rate, m/s	0.5 – 2.5
Pressure drop (no dust), Pa	500 – 1500

In *moving-bed granular filters*, the granules move (slowly) through the filter chamber by gravity, either steadily or at intervals. Fresh granules are added continuously from above. Regeneration takes place in an external loop. This filtration method operates without interruption of the dirty-gas stream. Multichamber design for regeneration is thus unnecessary.

Dust collection occurs mainly in the interior of the bed. Particles are transported to the filter granules by the same mechanisms as in fibrous depth filters: diffusion, inertial forces, and (less often) electrostatic attraction (cf. Section 5.2.2). For successful collection, the particles must adhere to the granules. Sieve effects become significant only after the deposition of sufficient dust and the formation of bridges or a cake.

Once a critical load or a critical pressure drop has been reached, dust can penetrate to the clean-gas side of the bed. With fixed beds, dust bridges can collapse; with moving granular beds, a danger exists that friction between granules will loosen collected dust particles, which will be carried out of the filter (reentrained).

Fluidized-bed granular filters have not gained a significant market share until now, but research continues.

5.4.3. Basic Designs

Fixed-Bed Filters. An example of a fixed-bed filter is the so-called *Drallschicht* (*DS*) *filter* shown in Figure 30 [61]. A cyclone-like precollector (b) removes coarse particles. Collection takes place as the gas flows downward through the bed (d). For regeneration, the dirty-gas stream is interrupted by adjusting the appropriate shutoff valve (e), causing clean gas to flow back through the bed while the bed is raked (g). Removed dust is collected partly in the hopper of the precollector and partly in another filter connected in parallel (multichamber design).

In the *granulate-tube filter* (Fig. 31), the granular filter material is contained in perforated double-wall pipes (c); the gas flows horizontally through the pipes. For regeneration (right-hand side of Fig. 31), the dirty-gas stream is again cut off. Purge gas sets the granules in motion and conveys them in a closed loop; at the same time, clean gas flows backward (horizontally) through

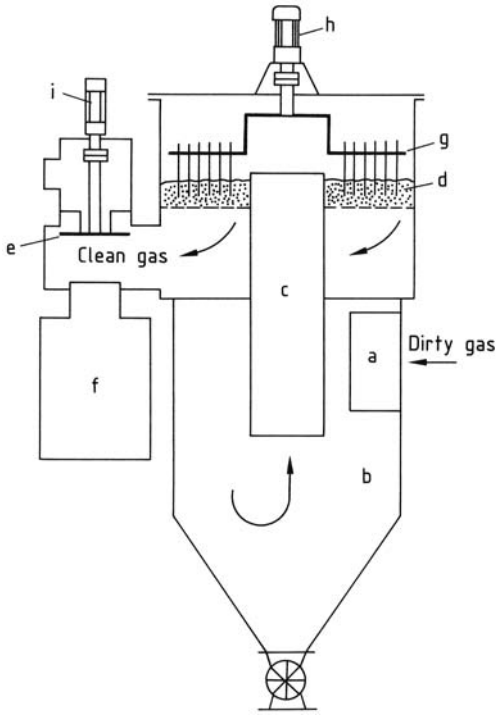

Figure 30. "Drallschichtfilter" in operation (Lurgi)
a) Tangential dirty-gas inlet; b) Precollector; c) Exit duct; d) Granular bed; e) Changeover valve; f) Clean-gas duct; g) Rake; h) Drive; i) Valve actuator motor

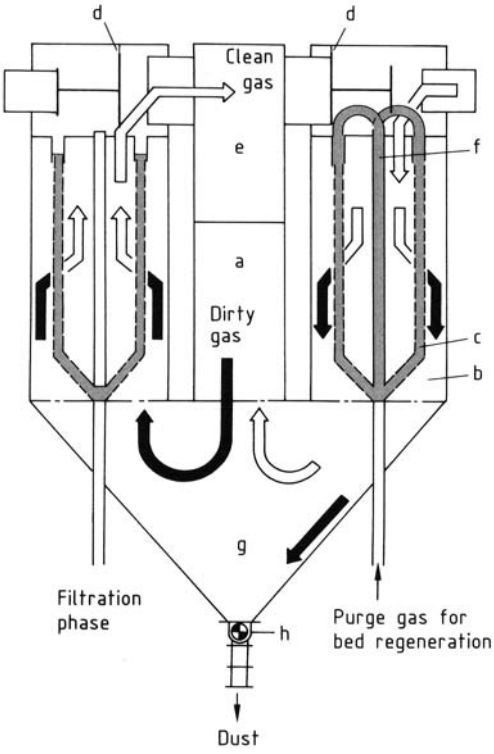

Figure 31. Granulate-tube filter (Lurgi)
a) Dirty-gas duct; b) Filter space; c) Perforated granulate tubes; d) Shutoff valve; e) Clean-gas duct; f) Riser pipe; g) Hopper; h) Screw conveyor

the pipes and carries the loosened dust to the hopper (g).

Moving-Bed Filters. An example of a moving-bed filter is the *countercurrent granular-bed filter* (Fig. 32). Gas and filter material move countercurrently. The dust content of the dirty gas is first lowered in a cyclone-like precollector. The gas then flows radially into the filter bed where it is redirected and slowed. The gas then flows upward through the fresh filter material (b) into the clean-gas plenum (a). To increase filtration area, the filter material is distributed in several conical containers stacked one above another; gas flows through these beds in parallel.

Dust-laden filter material is removed at intervals by a scraper (d), collected in the tube (c), regenerated externally in vibrating sieves, and returned to the top of the collector. This design and mode of operation make a multichamber device unnecessary.

5.4.4. Design Calculations

The design of granular-bed dust filters is mainly empirical (as in collection generally), and development of theories is not yet complete. However, existing formulas still yield valuable information about important variables and trends and, therefore, are discussed briefly. A detailed discussion can be found in [5].

5.4.4.1. Collection Efficiency

The initial fractional collection efficiency (no dust load in the bed) is described by

$$T(x) = 1 - \exp\left[-1.5\frac{(1-\varepsilon)}{\varepsilon} \cdot \frac{H}{d_G} \cdot \varphi(x)\right] \qquad (37)$$

where ε is the porosity of the bed, H is its height, d_G is the diameter of the filter granules, and $\varphi(x)$ is the single-granule collection efficiency.

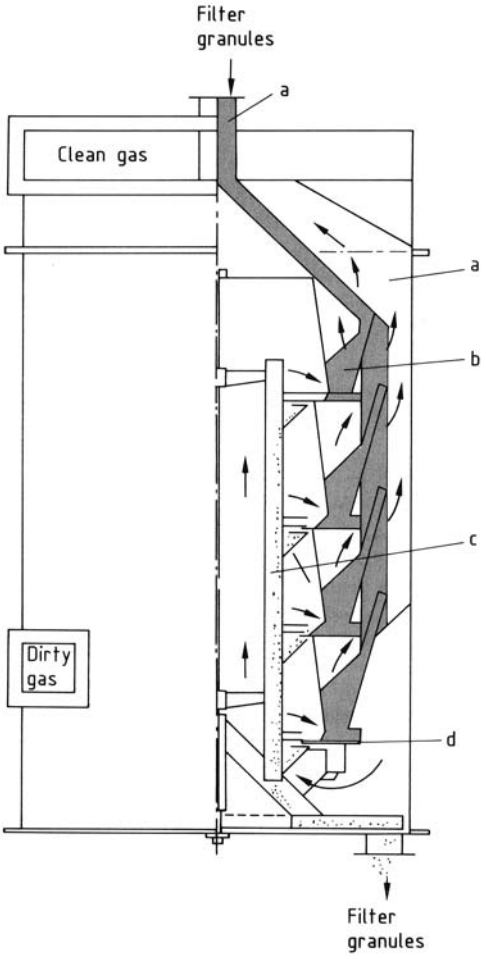

Figure 32. Vertical section of a countercurrent filter (Rüskamp)
a) Clean-gas plenum; b) Granular bed; c) Downpipe; d) Scraper
Arrows indicate direction of gas flow

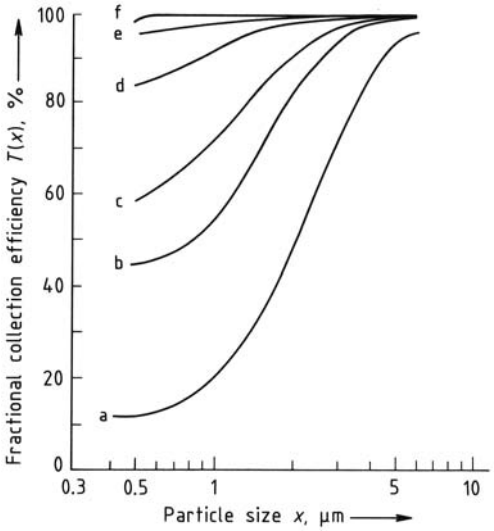

Figure 33. Fractional efficiency curves for a limestone bed (height 5 mm, granule diameter 0.28 mm) with various dust loads of quartz F 500 at a gas velocity of 0.055 m/s
Mass of dust W collected per unit filter area, g/m^2 (pressure drop Δp, Pa):
a) 0 (108, initial trial); b) 6.98 (117); c) 11.97 (141); d) 17.95 (244); e) 25.93 (452); f) 50.85 (1110)

The dependences of $T(x)$ on filter geometry (ε, H, d_G) have been confirmed experimentally [62, 63]. As the dust load in the bed increases, fractional efficiency increases, at least up to the critical load. The fractional efficiency curves in Figure 33 were measured with relatively small filter granules (d_G= 0.28 mm) and at low filtration velocities [64]. Under these conditions, the shift from collection in the bed to collection in the dust layer (i.e., to surface filtration) is relatively quick. As a result, fractional efficiencies are very high and only slightly dependent on particle size.

The difficulty in calculating fractional efficiency with Equation (37) is determination of the single-grain collection efficiency $\varphi(x)$. Transport mechanisms are the same as in fibrous-bed filters (diffusion, electrostatic attraction, inertia; see Section 5.2.2), but defining the flow field near a filter granule (which is assumed to be spherical) is more difficult.

Because the filter granules are close together, the flow fields derived for isolated spheres are too inexact, and correction factors are introduced to allow for the packing density [62]. At higher velocities, even flow fields modified in this way do not closely approximate reality.

The experimental fractional efficiency curves in Figure 34 essentially confirm theoretically predicted effects and trends. Below about 0.5 µm and 0.5 m/s (sodium chloride particles), diffusion effects are dominant. In this region, collection efficiency increases with decreasing particle size x, decreasing velocity U_0, and decreasing filter-granule size d_G. Inertial forces control collection to the right of the minimum (Quartz F 500), but here the curves pass through a maximum. The maximum shifts toward smaller particle sizes as the velocity increases, due to inadequate

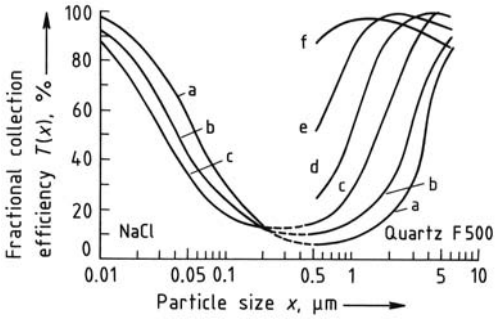

Figure 34. Fractional efficiency curves for a bed of glass beads at various filtration velocities
Bed height $H = 20$ mm; bead diameter $d_G = 0.58$ mm
Filtration velocity U_0, m/s:
a) 0.05; b) 0.10; c) 0.25; d) 0.5; e) 1.0; 1.5

adhesion of particles when they collide with the filter granules. This phenomenon still occurs in much thicker beds and becomes even more evident if Equation (37) is used to calculate the single-grain efficiency from measured fractional efficiencies [63]. These tests, performed on beds up to 9.7 cm thick and composed of 4-mm spheres, show that the dust particles bounce off at velocities as low as 2 m/s.

5.4.4.2. Pressure Drop

The pressure drop across the granular bed in its initial unloaded state can be calculated fairly accurately. Ergun's equation is used primarily because it holds for all Reynolds numbers and has been tested for granular beds.

$$\Delta p = 150\frac{(1-\varepsilon)^2}{\varepsilon^3}\cdot\frac{\mu_g\cdot U_0}{d_G^2}H + 1.75\frac{(1-\varepsilon)}{\varepsilon^3}\cdot\frac{\varrho_g\cdot U_0^2}{d_G}H \quad (38)$$

where U_0 is the superficial velocity and μ_g is the gas viscosity. The marked dependence on porosity ε should be noted. Inaccuracy in the determination of ε strongly affects Δp.

The pressure drop increases with time due to incorporation of dust into the bed. This process has been described by a few equations which apply only to special cases and are not generally valid. Accordingly, the time-dependent behavior of the pressure drop must be determined experimentally.

6. Electrical Precipitators

6.1. General

An especially efficient way of separating particles from gases is based on the forces exerted on charged particles in an electric field. This principle is important when inertial forces are no longer effective, i.e., for fine particles with a diameter of ca. < 1 µm. The benefits of such processes have been known and patented for over a hundred years. Large-scale implementation, however, did not start until early in the 20th century, when sufficiently powerful high-voltage equipment was developed. The developmental history, principles, and current status of this field have been described in detail [2, 5, 65–67].

Electrical collectors are often simply called *electrofilters;* the term *electrostatic precipitator* has been adopted even though the processes are by no means electrostatic and sizable electric currents are involved.

Because the required capital investment is rather large, the main application of these precipitators is in dust removal from large gas streams (up to several million cubic meters per hour). These include flue gases from power plants and refuse incinerators (furnaces), cement plants (rotary kilns and mill drying), the iron and steel industry (blast furnaces and converters), foundries, nonferrous metal refineries (furnaces), expanded-clay aggregate plants, and chemical plants. Collection efficiencies over 99.9 % can be obtained. Emission levels lower than 10 mg/m^3 can be achieved if the dust properties are favorable. Pressure drops are generally very slight (< 500 Pa).

6.2. Mode of Operation

6.2.1. Principles

The collection principle used in electrical precipitators is depicted in Figure 35 and involves three successive steps:

1. charging of particles,
2. transport of particles to the collecting electrode, and
3. removal of particles gathered on the collecting electrode.

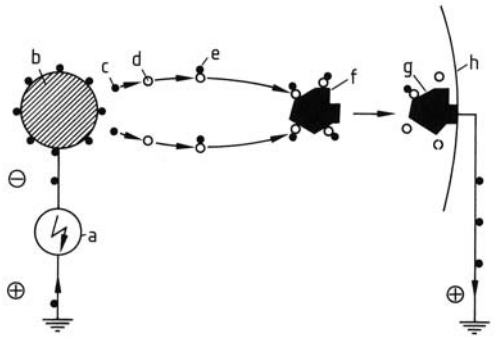

Figure 35. Schematic diagram of charging and collection process
a) High-voltage power supply; b) Emission electrode; c) Electron; d) Neutral molecule; e) Ionized molecule; f) Charged dust particle; g) Collected dust particle; h) Collecting electrode

Most particles carry an electrostatic charge, but it is usually too small for the collection process. Additional charge must, therefore, be supplied. This is accomplished by gas ions that are generated in a corona discharge. Figure 36 shows the configurations used for charging and collection: wire-in-tube (A) and parallel-plate (B and C) precipitators.

The parallel-plate types are by far more widely used and may be either two-stage or single-stage devices. In the two-stage unit (Fig. 36 B), the charging and collection regions are separate. These systems operate advantageously with a positive emission electrode and are preferably used in air-conditioning applications because a positive corona does not form ozone. However, the currents which can be obtained are not as high as with a negative corona. Higher currents are necessary for high collection efficiency and for operation with high dust concentration. Therefore, for dust removal from industrial exhaust gases, the single-stage negative-corona design is preferred (Fig. 36 C).

Typical voltages in industrial filters are 20 – 100 kV, with channel widths of 200 – 500 mm.

Electric charges released at the emission electrode attach themselves to the particles that are to be collected. The charged particles in the electric field between the emission and collecting electrodes are transported to the collecting electrode and retained. Liquid particles flow downward as a film, while solid particles form a dust layer that must be removed from time to time by rapping or flushing with a liquid. The loosened dust falls into a hopper beneath the collecting electrode. Dust removal is done on-line, i.e., the gas stream is not cut off. Consequently, previously collected dust can be reentrained and transported further. The collector length is therefore subdivided into several (three to six) successive zones, which are cleaned at different times in order to minimize dust penetration.

6.2.2. Charging of Particles

Production of Charge Carriers. The ions needed for particle charging are produced by corona discharge at the emission electrodes, which are made of thin wires or tapes with barbs. Triggering the corona discharge requires a minimum voltage, the *corona inception voltage,* which depends on the electrode geometry as well as the gas species and its properties; a typical value is in the range 10 – 30 kV.

If the applied voltage is raised, the current increases until electrical breakdown (sparking) occurs at the *breakdown voltage* (Fig. 37). The breakdown voltage depends on electrode geometry and gas properties. To obtain optimal

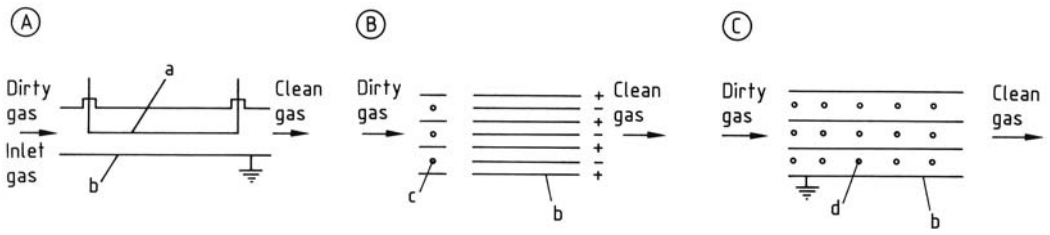

Figure 36. Schematic arrangements of emission and collecting electrodes in electrical precipitators
A) Wire-in-tube precipitator; B) Two-stage parallel-plate precipitator; C) Single-stage parallel-plate precipitator
a) Emission electrode; b) Collecting electrode; c) Positive emission electrode; d) Negative emission electrode

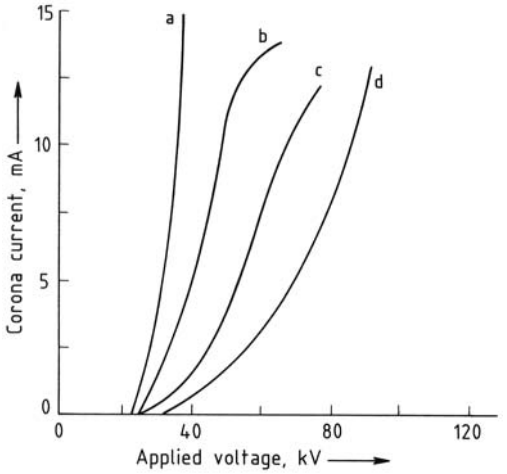

Figure 37. Current–voltage curve for a negative corona in nitrogen, nitrogen–oxygen mixtures, and air (electrical tube precipitator)
a) Nitrogen 100 %; b) Nitrogen 98 %, oxygen 2 %; c) Nitrogen 95 %, oxygen 5 %; d) Air

collection efficiencies, high field strengths and high corona currents are required. The d.c. voltage is, therefore, adjusted to establish a condition as close as possible to electrical breakdown. A trend is the use of pulsed voltage (pulse energization), in which the voltage peaks exceed the breakdown voltage [68].

To allow precipitator operation, the difference between the corona inception voltage and the breakdown voltage must not be too small. As the gas temperature increases, however, this difference becomes smaller and smaller, so that stable operation at atmospheric pressure (± 10 kPa) is difficult above ca. 400 °C. However, the difference becomes larger with increasing pressure; this point is especially important in cleaning gases from high-pressure fluidized-bed combustors: at pressures > 1 MPa, operation is possible even at 800 °C.

Attachment of Charge. Depending on particle size, the attachment of gas ions to particles occurs by one of two mechanisms: field charging or diffusion charging.

Field Charging dominates in the particle-size range above ca. 1 μm. The ions move toward the collecting electrodes along the electric field lines. As they move, the ions collide with particles and become attached to them. The charging process is time-dependent; 80 % of the maximum charge is acquired after about 0.1 s. The maximum charge is proportional to the surface area of the particle, i.e., to x^2. For a 2-μm particle, this amounts to some 250 elementary charges.

Diffusion Carging results from random thermal motion of the ions (Brownian motion) and is important chiefly for particles smaller than 1 μm. This process is slower than field charging: acquisition of 80 % of the maximum charge takes approximately 1 s. In this range, the maximum charge is proportional to the particle size x.

6.2.3. Effect of Dust Resistivity

Charged particles are transported to the collecting electrode and must adhere to it. The electrical properties of the particles, particularly resistance, are important for the behavior of both the particle on impact and the resulting dust layer.

The favorable range of resistivity for collection is $10^4 - 10^{11}$ Ω cm. Particles with a lower resistance ($< 10^4$ Ω cm) give up their charge quickly when they collide with the collecting electrode; they change their polarity and are repelled from the electrode back into the gas stream. If the resistance is too high ($> 10^{11}$ Ω cm), the particles form a layer that continues to accumulate more charge, thus leading to a weakening of the electric field and "reemission." Reemission results from discharge in the porous dust layer (back corona).

Dust resistivity depends on the geometry of the dust layer, particle characteristics, and gas properties (especially the dew point, Fig. 38); thus it should be measured under conditions as close as possible to those used in practice. The resistivity is made up of two contributions, surface resistivity and volume resistivity, which both depend on temperature but in opposite ways. The temperature–resistance curves therefore have a maximum (Fig. 38).

The resistivity of fly-ash particles is affected by their sulfur content. Some coals are so low in sulfur that the resulting fly-ash dust has a high resistance, which makes successful precipitator operation difficult. Consequently, electrical precipitation has been abandoned in power plants fired with these coals and bag filters have been installed. Problems caused by high dust

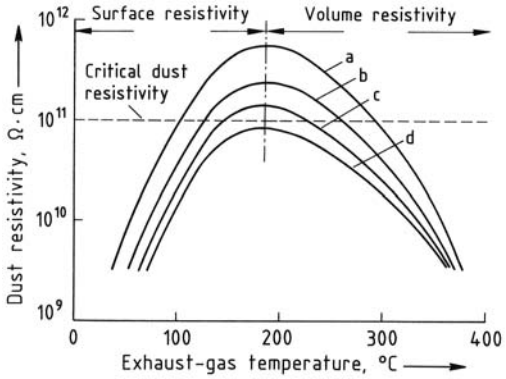

Figure 38. Electrical resistivity of dust particles as a function of temperature
Dew point of gas, °C:
a) 20; b) 40; c) 50; d) 60

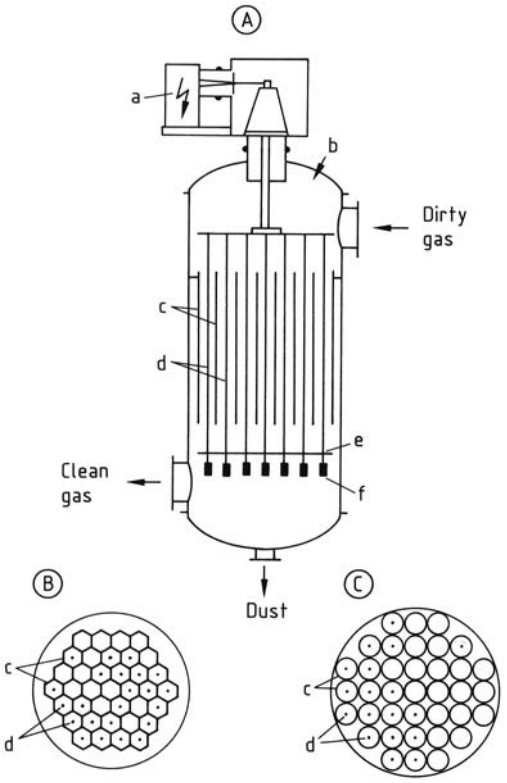

Figure 39. Tube precipitator consisting of individual collectors in parallel
A) Vertical section; B) Tubes with a hexagonal cross section (honeycomb precipitator); C) Tubes with a circular cross section
a) High-voltage power supply; b) Flushing; c) Tube walls (collectors); d) Emission electrodes; e) Electrode spacer; f) Weight

resistivity can be overcome through gas conditioning, e.g., by spraying water into the gas or adding sulfur trioxide in low concentrations. A sulfur trioxide level of 10 – 15 ppm has proved most suitable; it is completely adsorbed by the fly ash so that the sulfur oxide emission level does not increase [69]. Another way of promoting the collection of high-resistance dusts is the pulsed-voltage technique discussed in Section 6.2.2.

6.3. Basic Designs

Wire-in-tube Precipitators (Fig. 39) are employed for small quantities of gas and especially for the collection of liquids (e.g., tar mists and acid mists). The emission electrodes (wires) are stretched along the central axis of parallel tubes. The inside walls of the tubes serve as collecting electrodes. If the tubes are set up vertically, the collected liquid runs down the walls as a film. If solid particles are collected, they are frequently rinsed out by flushing the tubes with water. The tubes are usually 0.2 – 0.3 m in diameter and 2 – 5 m long. They may have a circular (Fig. 39 C) or a hexagonal cross section (Fig. 39 B). Since there is a conductive liquid film on the tubes, plastics such as PVC can be used instead of steel. This minimizes corrosion problems.

Parallel-plate Precipitators contain many plane or profiled plates that are suspended at uniform intervals (200 – 500 mm) as collecting electrodes (Fig. 40). Gas flows horizontally in the channels between plates. Emission electrodes hang in the midplane between neighboring plates. Particle removal may be either dry or wet.

In *dry electrostatic precipitators,* the dust layer collected on the plates is removed periodically by rapping the plates with hammers; the dust falls into the hopper beneath the plates. The total plate length is divided into several (three to six) zones for two purposes: (1) dust reentrainment is reduced because the zones can be cleaned at different times; and (2) separate zone-by-zone power controls allow the voltage to be adjusted in accordance with dust concentration, which declines exponentially along the precipitator.

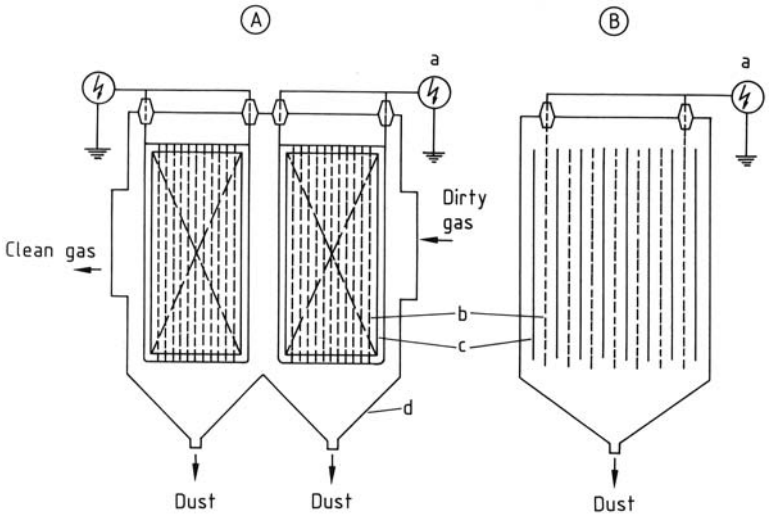

Figure 40. Schematic of a two-zone parallel-plate electrical precipitator
Vertical sections A and B are shown at right-angles to each other
a) High-voltage power supply; b) Emission electrode; c) Collecting electrode; d) Hopper

In *wet electrostatic precipitators,* the collecting electrodes are cleaned by flushing with water. The dust flows down off the plates with the water; reentrainment of the dust is thus effectively prevented.

If the dirty gas has a very high dust content, the corona or the electric field strength is weakened, i.e., collection performance deteriorates. Precollectors are then used to lower dust concentration. However, these should not significantly alter the particle-size distribution because dust removal from the plates is better with a wider distribution than with fine particles only. Simple deflecting vanes have proved suitable for this purpose [70].

If dust concentration in the clean gas must be particularly low, combinations of several types of dust collectors are employed: flue gases from blast furnaces can be cleaned up to 5 – 10 mg/m^3 by a series consisting of a cyclone, a scrubber, and a wet electrostatic precipitator.

6.4. Design Calculations

Calculations for precipitator design are concerned solely with collection efficiency; the very small pressure drop is not important.

In 1922, DEUTSCH derived the precipitator equation that bears his name. The equation has been challenged, but it is still used as the basis for sizing precipitators and for evaluating and interpreting measurements. If turbulent flow in the precipitator is assumed (i.e., the distributions of gas velocity and particle concentration transverse to the direction of flow are uniform) and if reentrainment and reemission are neglected, the Deutsch equation for fractional efficiency is

$$T(x) = 1 - \exp\left[-\frac{2 \cdot L}{a \cdot v} w(x)\right] \tag{39a}$$

where L is the collection length, a is the plate spacing (parallel plate precipitators) or the radius of the tube (tube precipitators), v is the gas velocity, and $w\,(x)$ is the so-called migration velocity. Equation (39) can also be written as

$$T(x) = 1 - \exp\left[-\frac{A}{\dot{V}} w(x)\right] \tag{39b}$$

where A is the surface area of the collecting electrodes and $\dot{V}$ is the volume gas flow rate. The ratio A/V is also called the specific collecting area.

The migration velocity $w\,(x)$ depends on the particle size and charge, the electric field, and the gas viscosity. It can be derived theoretically by solving the equation of particle motion [5]. In practice, migration velocity is calculated from the measured fractional efficiencies, by means of Equation (39a), (39b); it often lies in the range of 10 – 30 cm/s. The parameter $w\,(x)$ is basically

a transport coefficient that characterizes particle transport to the collecting electrode; it is thus vital for sizing electrical precipitators. Deutsch's assumption that w (x) is constant along the precipitator has not been confirmed experimentally [71]. The mean value of w (the effective migration velocity), recalculated with Equation (39a), (39b) from measured fractional efficiencies, increases with gas velocity and channel width [72]. The physical significance of these phenomena and their incorporation in the design equation are not yet completely understood because particle behavior inside the precipitator is still not clear. For this reason, the search for an optimal channel width has led to differing results in the range of 20 – 60 cm.

Nevertheless, Deutsch's equation continues to be of central importance in design. A variety of correction factors in the exponent of Equation (39a), (39b) have been suggested [73]. One problem in interpreting experimental studies is that measurements usually yield overall collection efficiencies, not fractional efficiency curves. The resulting w values thus represent integral mean values, which depend on particle-size distribution. As the distribution in the dirty gas becomes broader, the overall efficiency for a given precipitator declines. As one of the few fractional measurements shows, the shape of the fractional efficiency curve is rather complicated but also informative (Fig. 41) [74]. The ascending part of the curve, to the left of the minimum at ca. 0.4 μm, can be accounted for by the dependence on flow resistance of particle motion relative to the gas (Cunningham correction). The decline of the curve past ca. 3 μm has been explained by the typical behavior of incompletely combusted coal particles, which are repelled from the collecting electrode because of their low resistivity (cf. Section 6.2.3).

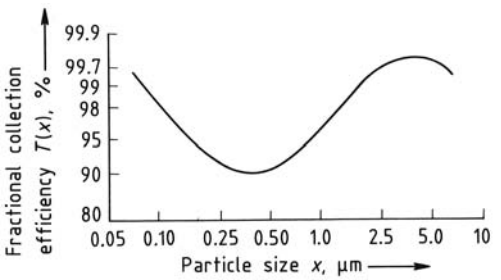

Figure 41. Experimentally determined fractional efficiency curve for an electrical precipitator (specific collecting area = 70 m^2 s m^{-3}) [74]

Improved particle measuring instruments have been developed recently; their use in determining particle motion and fractional efficiency curves for electrostatic precipitators should contribute to the understanding of this and other processes [75].

References

General References

1 F. Baum: *Luftreinhaltung in der Praxis*, Oldenbourg Verlag, München 1988.
2 H. Brauer (ed.): *Handbuch des Umweltschutzes und der Umweltschutztechnik*, vol. 3, Springer Verlag, Heidelberg 1996.
3 F. A. L. Dullien: *Introduction to Industrial Gas Cleaning*, Academic Press, San Diego 1989.
4 W. Licht: *Air Pollution Control Engineering*, 2nd ed., Marcel Dekker, New York 1988.
5 F. Löffler: *Staubabscheiden*, Thieme Verlag, Stuttgart 1988.
6 A. Ogawa: *Separation of Particles from Air and Gases*, vol. 2, CRC Press, Boca Raton, FL 1984.
7 E. Schmidt *et al.* (ed.): *High Temperature Gas Cleaning*, Institut für Mechanische Verfahrenstechnik und Mechanik, Karlsruhe 1996.
8 J. Seville: *Gas Cleaning in Demanding Applications*, Blackie, London 1997.

Specific References

9 Technische Anleitung zur Reinhaltung der Luft (TA Luft) 2002, Allgemeine Verwaltungsschrift zum Bundesimmissionsschutzgesetz.
10 DIN ISO 9276-4, Characterization of a Classification Process, 2006.
11 R. H. Perry, D. W. Green (eds.): *Perry's Chemical Engineers' Handbook*, 7th ed., McGraw-Hill, New York 1997.
12 M. Morweiser: Einfluss von Druck und Temperatur auf Trenngrad und Druckverlust von Aerozyklonen, TU Braunschweig, 1998.
13 VDI-Richtlinie 3676, Massenkraftabscheider (Inertial Separators), Beuth Verlag, Berlin 1999.
14 M. Bohnet, *Chem. Ing.-Tech.* **54** (1982) 621 – 630.
15 F. Boysan, W. H. Ayers, J. Swithenbank, *Trans. Inst. Chem. Eng.* **60** (1982) 222 – 232.
16 R. Kirch: *Der Einfluß der Turbulenz auf die Partikelbewegung im Gaszyklon*, VDI Verlag, Düsseldorf 1988.
17 VDI-GVC (ed.): "Zyklone zum Abscheiden fester Partikeln aus Gasen", *VDI-Wärmeatlas*, 10th ed., Springer, Berlin 2006.
18 D. Leith, W. Licht, *AIChE Symp. Ser.* **68** (1972) 196 – 206.
19 W. Barth, *Brennst. Wärme Kraft* **8** (1956) 1 – 9.

20 E. Muschelknautz, *Chem. Ing. Tech.* **44** (1972) 63 – 71.
21 P. W. Dietz, *Powder Technol.* **31** (1982) 221 – 226.
22 H. Mothes, F. Löffler, *Chem. Eng. Process* **18** (1984) 323 – 331.
23 T. Lorenz: *Heißgasentstaubung mit Zyklonen*, VDI-Verlag, Düsseldorf 1994.
24 P. Meißner, F. Löffler, VDI Ber. **294** (1978) 69 – 75.
25 W. Rentschler: *Abscheidung und Druckverlust des Gaszyklons in Abhängigkeit von der Staubbeladung*, VDI-Verlag, Düsseldorf 1991.
26 E. Schmidt, C. Wadenpohl, F. Löffler, *Chem. Ing. Tech.* **64** (1992) 76 – 78.
27 H. Rumpf, K. Borho, H. Reichert, *Chem. Ing. Tech.* **40** (1968) 1072 – 1082.
28 M. Bohnet, *Chem. Ing. Tech.* **56** (1984) 416 – 417.
29 W. Krambrock, *Chem. Ing. Tech.* **51** (1979) 493 – 496.
30 VDI-Richtlinie 3679, Naßabscheider für partikelförmige Stoffe (Wet separators for particle collection), Beuth Verlag, Berlin 1998.
31 K. Holzer, *Staub Reinh. Luft* **34** (1974) 361 – 365.
32 K. Holzer, *Chem. Ing. Tech.* **51** (1979) 200 – 207.
33 M. Wicke: *Aufbau, Leistung und Betriebsverhalten von Naßentstaubern*, VDI-Verlag, Düsseldorf 1970.
34 F. Ebert, H. Büttner, Proc. 1. World Congr. PARTEC, Nürnberg (1986).
35 F. Löffler, G. Schuch, *Filtr. Sep.* **18** (1981) 70 – 74.
36 W. Barth, *Staub Reinh. Luft* **19** (1959) 175 – 180.
37 S. Calvert, *J. A. P. C. A.* **24** (1974) 929 – 934.
38 G. Schuch, F. Löffler, *Verfahrenstechnik Mainz* **12** (1978) 302 – 306.
39 M. Schmidt, Dissertation Universität Karlsruhe, 1993.
40 C.-D. Schegk, F. Löffler, *Chem. Ing. Tech.* **59** (1987) 319 – 322.
41 S. Ripperger, G. Dau, *VT Verfahrenstechnik* **14** (1980) 164 – 168.
42 K. T. Semrau, *Chem. Eng.* **26** (1977) 87 – 91.
43 A. Bürkholz: *Droplet Separation*, VCH Verlagsgesellschaft, Weinheim, Germany 1989.
44 R. C. Brown: *Air Filtration*, Pergamon Press, Oxford 1993.
45 R. P. Donovan: *Fabric Filtration for Combustion Sources*, Dekker, New York 1985.
46 E. Schmidt: *Abscheidung von Partikeln aus Gasen mit Oberflächenfiltern*, VDI-Verlag, Düsseldorf 1998.
47 DIN-EN 1822, High-Efficiency Particulate Air Filters (HEPA and ULPA), 1998.
48 H.-J. Rembor: *Das Verhalten von Tiefenfiltern bei zunehmender Beladung*, Shaker Verlag, Aachen 2001.
49 C. N. Davies: *Air Filtration*, Academic Press, London 1973.
50 R. Hiller: *Der Einfluß von Partikelstoß und Partikelhaftung auf die Abscheidung in Faserfiltern*, VDI-Verlag, Düsseldorf 1981.
51 H. Baumgartner: Elektretfaserschichten für die Aerosolfiltration, VDI-Verlag, Düsseldorf 1987.
52 H. Baumgartner, F. Löffler, H. Umhauer, *JEEE Trans. Electr. Ins.* **21** (1986) no. 3, 477 – 486.
53 R. Maus: *Verhalten von Bioaerosolen bei der Abscheidung in Tiefenfiltern*, Shaker Verlag, Aachen 1997.
54 H. Jodeit: *Untersuchungen zur Partikelabscheidung in technischen Tiefenfiltern*, VDI-Verlag, Düsseldorf 1985.
55 E. Schweers: *Einfluß der Filterstruktur auf das Filtrationsverhalten von Tiefenfiltern*, VDI-Verlag, Düsseldorf 1993.
56 M. Lehmann: Untersuchungen zur Struktur und zur Beladungskinetik von Tiefenfiltern, Universität Karlsruhe, 2005.
57 F. Löffler, H. Dietrich, W. Flatt: *Dust Collection with Bag Filters and Envelope Filters*, Vieweg, Braunschweig 1988.
58 VDI-Richtlinie 3677, Filternde Abscheider, (Filtering Separators), Beuth-Verlag, Berlin, 1997.
59 E. Schmidt, B. Weiß, *Gefahrstoffe-Reinhalt. Luft* **58** (1998) 35 – 40.
60 E. Schmidt, T. Pilz, *Filtr. Sep.* **33** (1996) 409 – 415.
61 G. L. Kinchett, *Filtr. Sep.* **22** (1985) 378 – 380.
62 G. J. Tardos, N. Abuaf, C. Gutfinger, *J. Air Pollut. Control Assoc.* **28** (1978) 354 – 363.
63 S. L. Goren, T. D'Ottavio, *Aerosol Sci. Technol.* **2** (1983) 91 – 108.
64 W. Peukert, F. Löffler, Proceedings of International Conference on Advanced Coal Power Plant Technology, Düsseldorf, 2 – 4 Dec. 1987.
65 J. Böhm: *Electrostatic Precipitation*, Elsevier, Amsterdam 1982.
66 VDI-Richtlinie 3678, Elektrische Abscheider (Electrostatic Precipitators), Beuth-Verlag, Berlin, 1998.
67 K. R. Parker: *Applied Electrostatic Precipitation*, Blackie, London 1997.
68 K. Darby, *2nd Int. Conf. Electr. Precipitation*, Kyoto 1984, pp. 575 – 584.
69 G. Mayer-Schwinning, R. Rennhack, *Chem. Ing. Tech.* **52** (1980) 375 – 383.
70 K. Arras, *Zem. Kalk Gips*, **29** (1976) 241 – 247.
71 K. Kinkelin, *Fortschr. Ber. VDI Z. Reihe 15*, **24** (1982) .
72 H. Wiggers, *Staub Reinhalt. Luft* **42** (1982) 292 – 294.
73 G. Cooperman, *Atmos. Environ.* **14** (1984) 277 – 285.
74 S. Maartmann, *Staub Reinhalt. Luft* **34** (1974) 353 – 355.
75 H.-J. Schmid: *Zum Partikeltransport in Elektrischen Abscheidern*, Shaker Verlag, Aachen 1999.

Further Reading

A. C. Hoffmann, L. E. Stein: *Gas Cyclones and Swirl Tubes*, 2. ed., Springer, Berlin 2008.
H. Masuda, K. Higashitani, H. Yoshida (eds.): *Powder Technology*, CRC Press, Boca Raton 2007.
P. Patnaik: *Handbook of Environmental Analysis*, 2nd ed., Taylor & Francis, Boca Raton 2010.
R. H. Perry, D. W. Green (eds.): *Perry's Chemical Engineers' Handbook*, 8. ed., McGraw-Hill, New York 2008.
T. Salthammer, E. Uhde (eds.): *Organic Indoor Air Pollutants*, 2. ed., Wiley-VCH, Weinheim 2009.
K. Sutherland: *Filters and Filtration Handbook*, 5. ed., Elsevier Butterworth-Heinemann, Amsterdam 2008.
D. A. Vallero: *Fundamentals of Air Pollution*, 4. ed., Elsevier Acad. Press, Amsterdam 2008.